Full-scale increased iron dosage to stimulate the formation of vivianite and its recovery from digested sewage sludge

Prot, T.; Wijdeveld, W.; Eshun, L. Ekua; Dugulan, A. I.; Goubitz, K.; Korving, L.; Van Loosdrecht, M. C.M.

DOI
10.1016/j.watres.2020.115911

Publication date
2020

Document Version
Final published version

Published in
Water Research

Citation (APA)
Prot, T., Wijdeveld, W., Eshun, L. E., Dugulan, A. I., Goubitz, K., Korving, L., & Van Loosdrecht, M. C. M. (2020). Full-scale increased iron dosage to stimulate the formation of vivianite and its recovery from digested sewage sludge. *Water Research*, *182*, Article 115911. https://doi.org/10.1016/j.watres.2020.115911

Water Research 182 (2020) 115911

Contents lists available at ScienceDirect

Water Research

journal homepage: www.elsevier.com/locate/watres

Full-scale increased iron dosage to stimulate the formation of vivianite and its recovery from digested sewage sludge

T. Prot [a, b, *], W. Wijdeveld [a], L. Ekua Eshun [a], A.I. Dugulan [c], K. Goubitz [c], L. Korving [a], M.C.M. Van Loosdrecht [b]

[a] Wetsus, European Centre Of Excellence for Sustainable Water Technology, Oostergoweg 9, 8911, MA, Leeuwarden, the Netherlands
[b] Dept. Biotechnology, Delft University of Technology, Van der Maasweg 9, 2629, HZ Delft, the Netherlands
[c] Fundamental Aspects Mat & Energy Group, Delft University of Technology, Mekelweg 15, 2629, JB Delft, the Netherlands

ARTICLE INFO

Article history:
Received 28 October 2019
Received in revised form
30 April 2020
Accepted 2 May 2020
Available online 15 May 2020

Keywords:
Phosphorus recovery
Waste water treatment plant (WWTP)
Magnetic recovery
Mössbauer spectroscopy
X-ray diffraction (XRD)
Iron sulphide

ABSTRACT

The recovery of phosphorus from secondary sources like sewage sludge is essential in a world suffering from resources depletion. Recent studies have demonstrated that phosphorus can be magnetically recovered as vivianite ($Fe(II)_3(PO_4)_2*8H_2O$) from the digested sludge (DS) of Waste Water Treatment Plants (WWTP) dosing iron. To study the production of vivianite in digested sludge, the quantity of Fe dosed at the WWTP of Nieuwveer (The Netherlands) was increased (from 0.83 to 1.53 kg Fe/kg P in the influent), and the possible benefits for the functioning of the WWTP were evaluated. Higher Fe dosing is not only relevant for P-recovery, but also for maximal recovery of organics from influent for e.g. biogas production. The share of phosphorus present as vivianite in the DS increased from 20% to 50% after the increase in Fe dosing, making more phosphorus available for future magnetic recovery. This increase was directly proportional to the increase of Fe in DS, suggesting that vivianite could be favored not only thermodynamically, but also kinetically. Interestingly, analyses suggest that several types of vivianite are formed in the WWTP, and could differ in their purity, oxidation state or crystallinity. These differences could have an impact on the subsequent magnetic separation. Following the Fe dosing increase, P in the effluent and H_2S in the biogas both decreased: 1.28 to 0.42 ppm for P and 26 to 8 ppm for H_2S. No negative impact on the nitrogen removal, biogas production, COD removal or dewaterability was observed. Since quantification of vivianite in DS is complicated, previous studies were reviewed and we proposed a more accurate Mössbauer spectroscopy analysis and fitting for sludge samples. This study is important from a P recovery point of view, but also because iron addition can play a crucial role in future resource recovery wastewater facilities.

1. Introduction

Phosphorus (P) is an essential nutrient for all living organisms and is a key element for global food production as it is widely used as fertilizer (Childers et al., 2011). Currently, the raw material for its production is mined phosphate rock. Unfortunately, the resources are scarce and concentrated in a few countries (Morocco holds 70% of the P-rock), which makes phosphorus a vulnerable resource (Cordell et al., 2015). This situation creates the need to exploit secondary sources of phosphorus like manure or sewage sludge (Ohtake et al., 2019).

The phosphorus present in wastewater is normally removed at the waste water treatment plant (WWTP). The most popular P-removal strategies are enhanced biological phosphorus removal (EBPR) and chemical phosphorus removal (CPR). The first relies on phosphate accumulating organisms, while the second involves iron dosing or, more rarely, aluminum dosing (Morse et al., 1998). While phosphorus removal technologies are well-established and widely applied, phosphorus recovery remains a challenge (Wilfert et al., 2015). Currently, the two main recovery routes are via struvite precipitation for WWTPs using EBPR, and after incineration for those using CPR. However, both methods have limitations: the P-recovery percentage is low for the former one (Cornel et al., 2009) and infrastructure costs are high for the second (Desmidt et al., 2015).

* Corresponding author. Wetsus, European Centre Of Excellence for Sustainable Water Technology, Oostergoweg 9, 8911, MA, Leeuwarden, the Netherlands.
E-mail address: Thomas.prot@wetsus.nl (T. Prot).

https://doi.org/10.1016/j.watres.2020.115911

Recent studies indicate that the mineral vivianite ($Fe(II)_3(PO_4)_3*8H_2O$) is an important P sink in the digested sludge from CPR plants (Wilfert et al., 2016, 2018). Our team has demonstrated that the magnetic extraction of vivianite from DS is possible at lab-scale, opening a possible new route for P recovery (Prot et al., 2019). Wilfert et al., (2018) suggest that higher Fe dosing could increase the conversion of the P in sludge into vivianite, increasing the share of magnetically recoverable P.

Besides its possible effect on vivianite production, increased Fe dosing is in line with current trends in wastewater treatment. Northern European countries such as the UK and Germany have fixed low limits for P in WWTP effluent (0.15–0.3 ppm) that may decrease even further in the future (European Sustainable Phosphorus Platform, 2019). Such low P levels can only be achieved by CPR, usually by using Fe salts (Suresh Kumar et al., 2019). Moreover, Fe addition to the primary settler or the A-stage of a WWTP enhances the production of primary sludge, thus giving higher biogas yield after digestion (Li et al., 2005). It appears that the use of Fe in wastewater treatment fits in a future of net energy producing plants.

To verify the hypothesis of Wilfert et al., a controlled Fe dosing increase was realized to investigate the actual effect of the Fe dosing on vivianite production. To achieve this, the Fe dosing was doubled at the Nieuwveer WWTP (The Netherlands), and the results are presented in this article. Special attention is given to the impact of the higher Fe dosing on the integral parameters of the WWTP (e.g. P level in effluent, biogas production and N removal) to ensure that vivianite production is not achieved to the detriment of the WWTP's primary objectives, and in the scope of future wastewater treatment.

2. Materials and methods

2.1. WWTP and Fe dosing

The study took place at the AB plant in Nieuwveer (The Netherlands) (influent: 69.77m^3/day in 2018). There, a FeSO4 solution is dosed in the aerated A-stage for P and COD removal. The Solid Retention Times (SRTs) are 0.72 day for the A-stage, 13 days for the B-stage and 20 days for the anaerobic digester. This WWTP receives external sludge from other WWTPs at irregular intervals. The external sludges are mixed with the A and B sludges before being thickened and fed to the digester. The external sludge accounts for ~30% of the total sludge volume.

To study the influence of the Fe dosing increase, the quantity of $FeSO_4$ dosed in the A-stage was doubled for 4 months. The dosing can be broken down into 3 phases, as shown in Fig. 1. The phase II with the highest Fe dosing will be the studied period.

2.2. Sample handling

Four samples were taken every two weeks from the sludge line: the settled sludge from A-stage, the settled sludge from B-stage, the mixed A-stage, B-stage and external sludge (MS) before digestion and the digested sludge (Appendix A). The sludge line was sampled twice in phase I, before the start of the Fe dosing as a reference and once in phase III. Eight other samples were taken at regular intervals for 4 months; after which time a steady-state should be reached in all the units (Appendix A). Samples were poured to the brim into air-tight polyethylene bottles and stored in a 4 °C fridge after 4 h of transportation. At Nieuwveer, 1–2 mL of each sample was immediately filtered (0.45 μm filter) and fixed with 0.05 mL of 0.5M HCl to prevent Fe oxidation. These samples were analyzed with the ferrozine method for Fe speciation and ICP-OES for elemental composition. Sludge samples were centrifuged for 15 min at 3750 rpm. The cake was dried at 25 °C in a fume hood for 48h for Total Solid (TS) measurement and later ground and digested for elemental composition and SEM-EDX. A part of the cake of the DS was dried in a glove box under anaerobic and light-free conditions to prevent vivianite oxidation for XRD (X-Ray Diffraction) and Mössbauer spectroscopy analysis. The drying of the sludge was done at room temperature to avoid the decomposition of vivianite.

2.3. Analyses

2.3.1. Light microscopy & SEM-EDX

Around 0.1g of dried solid samples were ground for light microscopy and SEM-EDX analysis. The grinding was done to break the organic matter shell covering the vivianite crystals that prevented proper microscope observation. The light microscope used was a Leica MZ95 equipped with a Leica DFC320 camera.

The SEM-EDX apparatus was a JEOL JSM-6480 LV Scanning Electron Microscope (SEM) equipped with an Oxford Instruments x-act SDD Energy Dispersive X-ray (EDX) spectrometer. The working distance was 10 mm for an accelerating voltage of 15.00 kV. Around 0.1g of dried samples were covered with a 10 nm-layer of gold using a JEOL JFC-1200 fine coater to make the surface electrically conductive. The software used was JEOL SEM Control User Interface for the SEM and Oxford Instruments Aztec for the EDX data processing.

2.3.2. XRD

After being dried in the dark in an anaerobic chamber, the samples were introduced in a 0.7 mm glass capillary under anaerobic conditions and minimum light exposure. The samples were kept and transported in a sealed sample holder covered with aluminum foil. Just before measurement, the capillaries were sealed with a burner. The device used was a PANalytical X'Pert PRO diffractometer with Cu-Ka radiation (5-80° 2θ, step size 0.008°). The peaks assignment was realized with the software Origin Pro 9.

2.3.3. Mössbauer spectroscopy

The samples were dried as explained in section 2.3.2 to prevent vivianite oxidation. Then, they were introduced in plastic rings sealed with Kapton foil and Epoxy glue to prevent oxygen exposure and wrapped in aluminum foil for light protection. The sample weight was adjusted to contain a maximum of 17.5 mg of Fe/cm^2. If the sample contained too much Fe, it was diluted with inert carbon powder. Transmission ^{57}Fe Mössbauer absorption spectra were collected at 300 K with a conventional constant-acceleration spectrometer using a^{57}Co (Rh) source. Velocity calibration was carried out using an α-Fe foil. The Mössbauer spectra were fitted using the Mosswinn 4.0 program (Klencsár, 1997).

2.3.4. Ferrozine method

First, 2 mL of sample was filtered and fixed with HCl 0.1 mL of 0.5M HCl directly at the WWTP to avoid Fe oxidation/reduction, and analyzed under anaerobic conditions 4h after sampling. The Fe speciation was determined using the ferrozine method, as explained in Viollier et al., (2000). In brief, 1 mL of HCl-fixed sample was added into a cuvette to 0.1 mL of a ferrozine solution, which forms a pink complex with Fe^{2+}. The absorbance was measured at 562 nm after 15 min of reaction with a Shimadzu UV-1800 Spectrophotometer. Then, 0.15 mL of 1.4 M hydroxylamine was added to 0.8 mL of the complexed solution to reduce all the Fe^{3+}. The reduction took place for 12h to ensure that all the organically bound Fe was reduced (Rasmussen and Nielsen, 1996). Finally, 0.05 mL of 10M acetate buffer was added to the sample, and the final absorbance was measured. The Fe^{2+} and Fe^{3+} were calculated using these 2 absorbances.

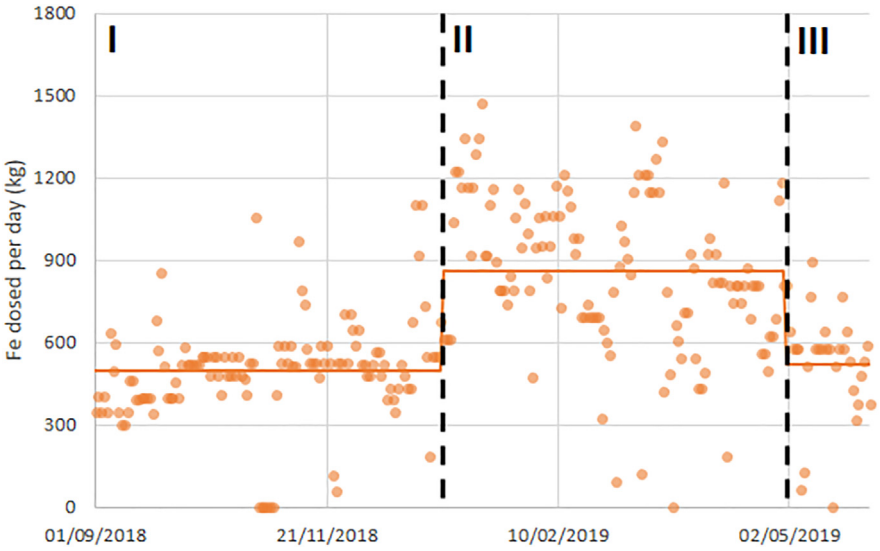

Fig. 1. Daily and average Fe dosing before (Phase I: 494 kg Fe/day), during (Phase II: 860 kg Fe/day), and after the study (Phase III: 520 kg Fe/day).

2.3.5. Microwave digestion & ICP-OES

Solid samples were destroyed in an Ethos Easy digester from Milestone equipped with an SK-15 High-Pressure Rotor. Around 50 mg of dried solid was introduced in a Teflon vessel in which 10 mL of ultrapure HNO_3 (64.5–70.5% from VWR Chemicals) was poured. The digester reached 200 °C in 15 min, was run at this temperature for 15 min, and was cooled down for 1h.

The elemental composition of the microwave digested samples and of the filtered samples were measured via Inductively Coupled Plasma (PerkinElmer, type Optima 5300 DV) equipped with an Optical Emission Spectroscopy (ICP-OES). An Autosampler, PerkinElmer, type ESI-SC-4 DX fast was used, and the data were processed with the software PerkinElmer WinLab32. The rinse and internal standard solution were respectively 2% of HNO_3 and 10 mg/L of Yttrium.

2.3.6. Global parameters of the WWTP

The following parameters of the WWTP were measured by the operators of Nieuwveer on-site:

- P effluent concentration (measured by Aquon according to the NEN norms)
- H_2S content in the biogas (measured by INCA 4000 T101 from Union Instruments GmbH)
- COD removal (measured by Aquon according to the NEN norms)
- Biogas production (measured by ST51-FR32C00A flow meter from Fluid Components International LLC)
- Nitrogen removal (measured by Aquon according to the NEN norms)

3. Results & discussion

Recovery of phosphorus via magnetic extraction of vivianite is a recent technique and is still in development. In Prot et al., 2019, we reached the first milestone by maximizing the quantity of P present as vivianite. The results of Wilfert et al., (2018) had suggested that an increase in Fe dosing could promote vivianite formation. However, they had conducted their study by examining sludge from 6 WWTPs with a fixed Fe/P ratio. To investigate the actual effect of the Fe dosing on the vivianite content in the DS (vivianite content, efficiency of the dosing, delay required to form vivianite), therefore, a controlled Fe dosing increase at a single WWTP is required.

The water authority Brabantse Delta made this research possible by increasing the iron dosing at the WWTP Nieuwveer (The Netherlands) from 0.83 to 1.53 kg Fe/kg P in the influent for a period of 4 months. The effect of this increase on phosphate behaviour and the integral operation of the treatment plant (e.g. P level in effluent, biogas production, COD removal …) was studied, and the results are discussed in this section. Since the strategy of recovering P as vivianite is novel, the analytical methods are still under development and subject to possible improvements. For this reason, the first part of the discussion is dedicated to the quantification of vivianite in digested sludge.

3.1. Quantification of vivianite in digested sludge: a short review and best practice

The major problem while studying vivianite in digested sludge is its quantification. Wilfert et al., (2018) used standard addition of synthetic vivianite together with XRD. A drawback of this method is its use of pure vivianite, even though the vivianite in sludge could be impure (Wilfert et al., 2016; Seitz et al., 1973). Moreover, XRD is unable to detect small or amorphous vivianite, which creates greater uncertainty. Despite these facts, XRD results were in line with Mössbauer results in their study, even though vivianite content was always estimated on the higher end with XRD.

Mössbauer spectroscopy can detect Fe minerals independently of their size or crystallinity and is considered to be the best technique for vivianite quantification so far. Yet, some discrepancies are present in the literature regarding sample handling and measuring, and data fitting. These problems will be discussed below, and an improved practice for vivianite determination with Mössbauer will be proposed. To understand the data fitting for Mössbauer spectroscopy, it is important to know that a crystalline unit of vivianite bears 3 possible positions for Fe: 1 octahedral site called site A and 2 equivalent octahedral sites called site B (Mori and Ito, 1950). The most characteristic feature of vivianite is that it has 2 doublets for Fe^{2+} present in site A (1 Fe^{2+} ion) and site B (2 Fe^{2+} ions). The Mössbauer parameters for these sites are well described and accepted in the literature: Site A (Isomer Shift (IS) = 1.2 ± 0.1 mm/s, Quadrupole Splitting (QS) = 2.4 ± 0.1 mm/s) and Site B (IS = 1.25 ± 0.1 mm/s, QS = 3.0 ± 0.1 mm/s) (McCammon et al.,

1980; Rouzies and Millet, 1993; Nembrini et al., 1983). Thus, the amount of Fe^{2+} present in vivianite in a sample can be reliably quantified.

However, vivianite can easily be oxidized by oxygen and/or light (Čermáková et al., 2013; McCammon et al., 1980) leading to the transformation of a part of the Fe^{2+} from both sites into Fe^{3+}. The signal of Fe^{3+} in vivianite is difficult to distinguish from that of Fe^{3+} species that can generally be present in sludge samples. Therefore, the samples are generally protected from oxidation as much as possible (Wilfert et al 2018; Wang et al., 2019, this study) to prevent/minimize the oxidation of Fe during sampling and handling. The samples can be studied by Mössbauer spectroscopy at temperature from 4.2K to 300K, although Wilfert et al. (2016, 2018) reported that measurements at 4.2K were not suitable for vivianite determination due to the complexity of the signal. Vivianite can be quantified at 100K (Wilfert et al., 2018; Wang et al., 2019), but these analyses do not seem to add any information compared to the quicker and easier analyses at 300K. Several researchers working with DS proposed measurements at 300K with a fitting with 3 doublets: Fe^{2+} in site A, Fe^{2+} in site B and Fe^{3+}/Fe^{II} accounting for all the Fe^{3+} species (including Fe^{3+} in vivianite) and low-spin Fe^{2+} compounds like pyrite (Prot et al., 2019; Frossard et al., 1997; Wilfert et al., 2018). Vivianite is likely to be partly oxidized in DS so its content was probably underestimated in these cases as the Fe^{3+} in the oxidized vivianite will not be taken into account.

To overcome the neglect of Fe^{3+} in the vivianite analysis, Rouzies and Millet (1993) proposed to fit the Fe^{3+} in vivianite with 3 additional doublets. Because our samples could not be fitted this way, we synthesized vivianite and let it oxidize for 15 days. The resulting spectra could be fitted with the 2 Fe^{2+} doublets of vivianite and one doublet (IS = 0.46 mm/s and QS = 0.63 mm/s) accounting for the oxidized Fe in vivianite (Table B1). These parameters are in line with those reported by McCammon et al., (1980), Nembrini et al., (1983) and Rouzies and Millet (1993) (averaging the 3 doublets proposed for Fe^{3+} in vivianite). The spectra of DS samples collected during the present study could successfully be fitted with 4 doublets: Fe^{2+} site A, Fe^{2+} site B, the proposed (IS = 0.46 mm/s and QS = 0.63 mm/s) doublet for Fe^{3+} in vivianite and a doublet accounting for the remaining Fe^{3+} and low-spin Fe^{2+}. With this fitting, the quasi-inevitable oxidation of vivianite doesn't lead to a constant underestimation of its content.

To summarize, the authors propose a strategy where samples do not necessarily need to be protected from oxidation and are measured at 300K. The spectra should be fitted with 4 doublets: Fe^{2+} site A (IS = 1.2 ± 0.1 mm/s, QS = 2.4 ± 0.1 mm/s), Fe^{2+} site B (IS = 1.25 ± 0.1 mm/s, QS = 3.0 ± 0.1 mm/s), Fe^{3+} in vivianite (IS = 0.46 mm/s and QS = 0.63 mm/s) and the remaining signal corresponding to other Fe^{3+} species low-spin Fe^{2+} like pyrite. These recommendations allow easier sample handling and higher accuracy of the vivianite quantification.

3.2. Effect of the higher Fe dosing on vivianite formation

3.2.1. Fe dosing increase promotes quick and efficient vivianite formation in DS

The primary objective of this study was to evaluate whether increased Fe dosing would effectively increase the proportion of vivianite present in DS, as suggested by Wilfert et al., (2018). Fig. 2 shows that the Fe content in DS increased over time from 40 mg/g until it reaches a steady-state at around 65–70 mg/g. Despite the doubling of the Fe dosed (494 kg/day in phase I to 860 kg/day in phase II), the Fe content in DS did not double. This may be the result of the mixing of on-site produced sludge with 30% of external sludge before digestion, which "dilutes" the Fe-rich produced sludge. It is important to verify that this Fe increase in the DS is accompanied by an increase of the vivianite content.

First of all, XRD confirmed the presence of vivianite in all the samples (Appendix A). Also, modelling using Visual Minteq showed that the Fe and P concentrations in the slude liquor are above the saturation index for vivianite (Appendix E). SEM-EDX analysis also showed particles with a sheets agglomerate structure, characteristic of vivianite, and an Fe/P ratio close to 1.5 (Fig. 3) (Zelibor et al., 1988; Rothe, 2016). The quantification of vivianite in the samples was performed according to the improved Mössbauer strategy described above. The results indicate that the vivianite content in DS increased from 50 to 150 mg/g of TS, following the increase of Fe in DS (Fig. 2). The fraction of P present as vivianite followed the same trend with an increase from 20% to 50% (Fig. 2). This confirms the main research hypothesis of this study: an increase in Fe dosing increases the proportion of P present as vivianite in DS.

Interestingly, the increase in vivianite immediately followed the increase in Fe content in sludge, indicating that the P present in digested sludge is quickly converted to vivianite. Nriagu et al., (1974) stated that vivianite is the most stable P mineral in a reducing environment (like DS). This result suggests that vivianite could also be kinetically favored.

To confirm that this vivianite formation technique is efficient, it is important to verify how much of the extra Fe dosed is actually used to form vivianite. Firstly, mass balances show that >99% of the Fe in the digested sludge can be found in the solid fraction (Appendix F). Secondly, data in Appendix G suggests that the content of Fe in vivianite increases linearly ($R^2 = 0.86$) with the Fe content in DS. The slope of this line is 1.24 ± 0.16, confirming that all the "extra" Fe present in DS was present as vivianite. Moreover, a slope bigger than 1 suggests that some of the Fe that was present in sludge in non-vivianite species was converted to vivianite as well. Such non-vivianite species could be Fe oxides, FeS_x or organically-bound Fe for example.

3.2.2. FeS compounds are forming prior to vivianite in digested sludge

The data obtained in this study follow the same trend observed in Wilfert et al., (2018) (Appendix H). The distribution of their data is broader since they used data from several studies, several plants, and different analytical methods and fitting. Their study showed that the fraction of P present as vivianite increased linearly with the Fe/P ratio and seemed to reach a plateau at Fe/P > 1.5, which is the ratio in pure vivianite, due to limited phosphorus availability. For lower Fe/P ratios, the absence of vivianite is likely related to the lower solubility product for ironsulfide. The data of Wilfert et al., (2018) would seem to suggest that a Fe/P ratio of around 0.2–0.4 would be needed before vivianite precipitation occured (x value for y = 0 in Appendix H). Our set of data suggests, however, that a value of 0.5–0.6 is required. We hypothesize that these discrepancies are mainly due to the strong influence of the S content in sludge, which needs to be consumed before any Fe is available for vivianite precipitation. This suggests that a comparison of data from different WWTPs would only be possible if the quantity of S were taken into account. Accordingly, a S-corrected Fe/P ratio was calculated in our study, assuming that all the S was formed as FeS before vivianite. Even though FeS_2 is the most stable inorganic Fe precipitate under anaerobic conditions (Pourbaix, 1963), pyritization is a slow process under the digester conditions (Nielsen et al., 2005). Therefore, the meta-stable amorphous FeS could be a precursor to the formation of pyrite (Morse et al., 1998; Dewil et al., 2009). This could explain why no trace of crystalline FeS_x has been found in our samples by XRD.

The percentage of phosphorus in vivianite was plotted as a function of the S-corrected Fe/P, with data from both studies

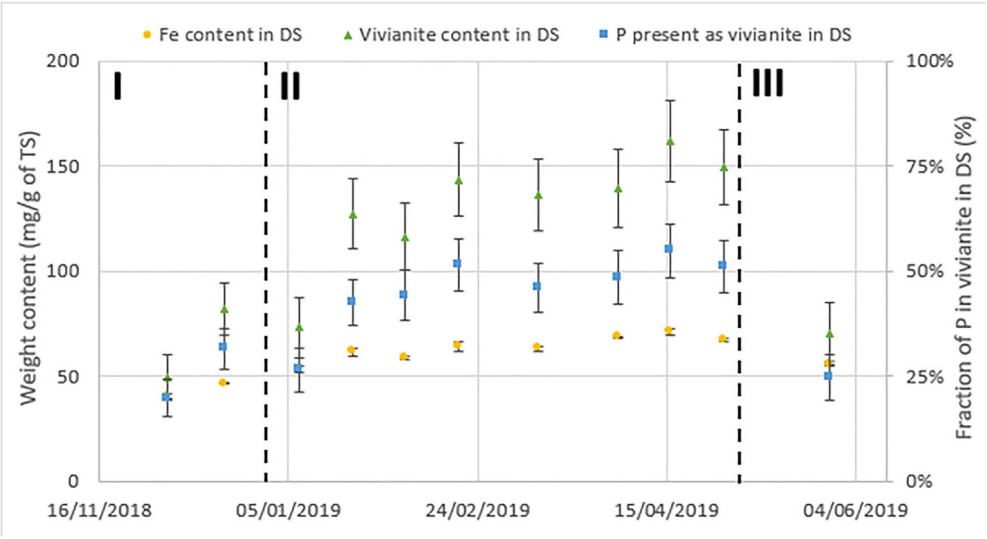

Fig. 2. Fe and vivianite content in the solid phase of the digested sludge of Nieuwveer (primary axis). Fraction of phosphorus in the solid phase of the digested sludge present as vivianite (secondary axis). (calculated from the Mössbauer results in Appendix B and the ICP-OES results in Appendix D). I, II and III correspond to the different Fe dosing phases as decribed in Fig. 1.

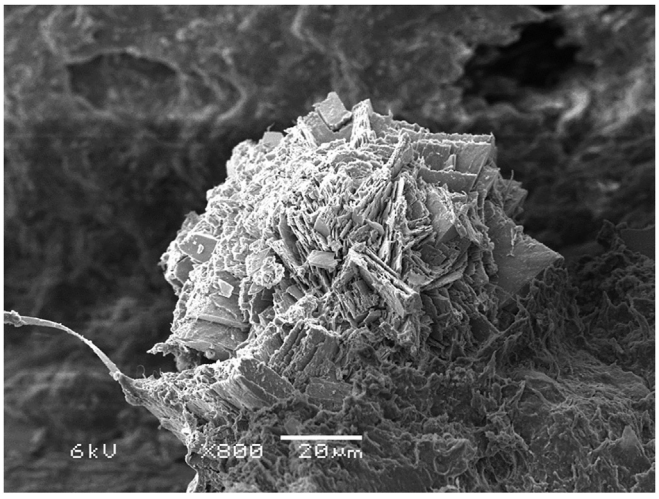

Fig. 3. Example of a vivianite particle found in the digested sludge (sample DS2) of Nieuwveer and observed by SEM.

presenting less variation ($R^2 = 0.86$ for S-corrected Fe/P in Fig. 4 and $R^2 = 0.76$ for uncorrected Fe/P in Fig. H1). This suggests that the discrepancies observed were indeed related to the different sulphide content. The data for the S-corrected Fe/P ratio between 0 and 1 follow a linear trend ($y = 1.01x-0.21/R^2 = 0.86$). This suggests that 100% of phosphorus will be present as vivianite for a S-corrected Fe/P ratio of 1.2, although this is contradicted by the data with Fe/P > 1 presented in Fig. 4. The proposed linear relation seems to be only valid for low S-corrected Fe/P ratio (from 0 to 1 the authors suggest). This is due to the fact that a fraction of the phosphorus could be organically bound or precipitated with calcium or as struvite. The intercept with the X-axis indicates that a S-corrected Fe/P ratio of 0.2 is needed before the formation of vivianite. This suggests not only that S competes for Fe, but that Fe is also depleted by another form before being available for vivianite precipitation. This part of the Fe could be present as amorphous Fe oxides/hydroxide (no crystalline FeO detected with XRD) and/or bound to humic substances (Abros'kina et al., 2016; Lovley et al., 1999). Thermodynamic modelling suggests that vivianite, FeS and iron oxides can form in the conditions of the Nieuwveer WWTP (Appendix E). Strengite is often mentioned as one of the possible FeP minerals in wastewater and could form according to our modelling results. However, no trace of it has been found by XRD or Mössbauer spectroscopy. Visual Minteq does not take into account some parameters (such as kinetics and activation energy) in its model, which can explain the discrepancies between the prediction and reality. For example, it is common that a mineral kinetically favored forms over a mineral thermodynamically favored (Brown et al., 1985). This could explain why strengite has never been found in previous studies within our group (Wilfert et al., 2015, 2018; Wang et al., 2019).

These observations lead to an important conclusion for WWTPs aiming to recover P via vivianite: the Fe dosage needs to be adapted according to the sulphur content present in the sludge. More specifically, Fe should be dosed in a molar ratio 1:1 compared to the S in DS before any vivianite can be found in DS. This extra Fe dosing required is not a waste as it will also help control H_2S emission (see 3.3). In most of cases, S would have already been bound by Fe, therefore, no extra Fe is needed to compensate for S if one wants to increase the vivianite content.

3.2.3. *There is evidence that different types of vivianite are formed*

Several results from the current study suggest that there are different kinds of vivianite formed in the WWTP at Nieuwveer. This finding is important since these vivianite species could have different properties, directly impacting their magnetic recovery. Different degrees of oxidation and impurity inclusion could lead to different types of vivianite. Indeed, vivianite can easily be oxidized by light and oxygen (Čermáková et al., 2013; McCammon et al., 1980), and Fe atoms in its structure can be replaced by other cations (Rothe et al., 2016; Seitz et al., 1973). Oxidation of vivianite and substitution of Fe by a non-magnetic cation (Mg^{2+}, Ca^{2+} …) modify the structure of vivianite (transition from crystalline to amorphous), and could impact its magnetic properties. Mössbauer results suggest that not all the vivianite formed in Nieuwveer is identical, but do not allow a clear conclusion to be drawn about their characteristics (detailed discussion in Appendix I).

In their study, Wilfert et al., (2018) used standard addition with

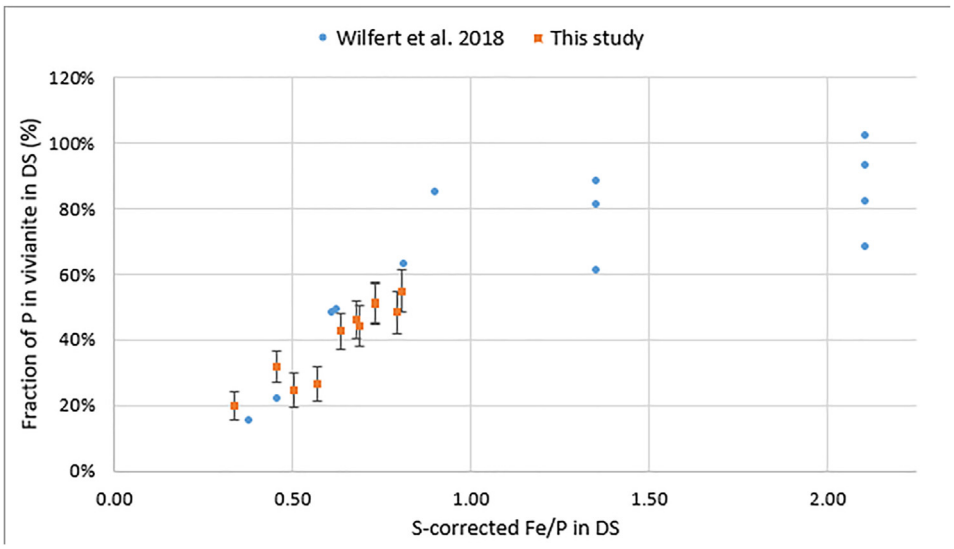

Fig. 4. Fraction of phosphorus in the solid phase of the digested sludge present as vivianite as a function of the S-corrected Fe/P molar ratio. Combined data from Wilfert et al., (2018) (6 different WWTPs) and the present study (calculation in Appendix H). The S-corrected Fe/P ratio was calculated assuming that Fe was first precipitating as FeS before vivianite. The data from Frossard et al., (1997) did not include S concentration, so were not included.

XRD to quantify vivianite in DS as the XRD signal should be proportional to the quantity of vivianite. However, in the current study, the XRD signal stays failry constant (Appendix I) despite an increase in vivianite content in sludge. This result is surprising and suggests that the newly formed vivianite is different. As XRD can not detect it, this other vivianite could be smaller or amorphous.

Light-microscope pictures of vivianite extracted from the DS at Nieuwveer showed that not all the vivianite particles are identical. A color gradient can be observed in Fig. 5, and hints that some particles are more oxidized than others. Colorless when non-oxidized, vivianite becomes bluer with a higher degree of oxidation (Zelibor et al., 1988; Ogorodova et al., 2017). The oxidation of vivianite is accompanied by the departure of a proton from the vivianite structure, destabilizing its crystalline matrix. However, due to the anaerobic conditions in the digester, it is unlikely that vivianite oxidizes in this environment. It is possible that the dark blue crystals formed in the early stages of the WWTP and were oxidized in the aerated zones. Wilfert et al., (2018) already observed vivianite formation before digestion in several WWTPs. Vivianite was also found in Nieuwveer in the B-stage and mixed sludge (Table B1). Almost all the soluble Fe in the A-stage was Fe^{2+}, giving favorable conditions for vivianite formation (SI~3) (Appendix E). In the B-stage, the concentration of Fe^{2+} was low (~0.2 ppm), creating a barely saturated environment for vivianite formation (SI around 0). This suggests that the vivianite identified in the B sludge either forms in the A-stage, and is transported to the B-stage afterward, or forms slowly in the B-stage. This early formed vivianite will have been in oxidative conditions for enough time to be oxidized (SRT for B-stage: 16 days in Nieuwveer).

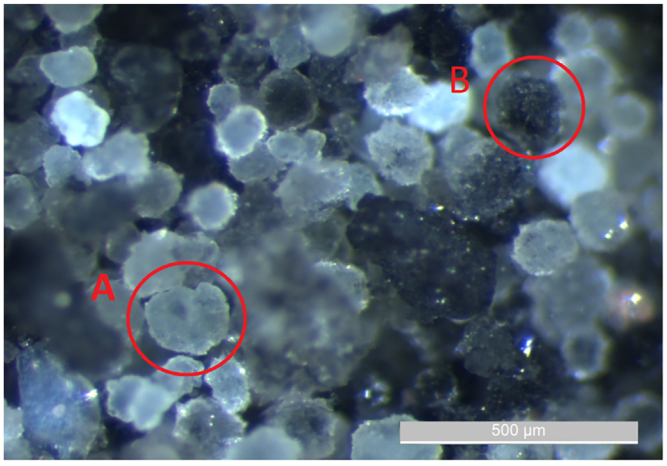

Fig. 5. Light-microscope picture of the vivianite extracted from the digested sludge from Nieuwveer with minimum oxygen and light exposure. This sample was magnetically separated at our pilot installation. Particle A: the light blue color suggest a small degree of oxidation (these particles turned dark blue after longer oxygen exposure). Particle B: the dark blue color suggests a high degree of oxidation.

To summarize, there is clear evidence that different types of vivianite formed in Nieuwveer, but we could not identify their characteristics with certainty. From the results, we hypothesize that some vivianite forms early in the WWTP and has different characteristics (oxidation level, crystallinity) than the vivianite forming under anaerobic conditions in the digester. It is crucial to further study these vivianite species and their properties since it may influence their magnetic recovery.

3.3. Impact of increased Fe dosing on the functioning of the WWTP

While increasing Fe dosing favors vivianite formation, which is significant in terms of phosphorus recovery, this should no happen to the detriment of the global functioning of the WWTP. In this regard, the following integral parameters of the Nieuwveer WWTP were monitored: P in the effluent, H_2S in the biogas, nitrogen removal, biogas production, COD removal and dewaterability of the sludge. Since WWTPs are influenced by seasonal effects, the comparison was made to years with normal Fe dosing, but for the same time period (period II: 01/01 to 30/04 as in Fig. 1).

First of all, total phosphorus concentrations in the effluent decreased after increasing the iron dosing. Fig. 6 shows that it was reduced to an average of 0.42 mg/L during the period of high Fe dosing, compared to an average of 1.28 mg P/L for the 4 previous years in the same period. Fe is dosed in the first place to remove phosphorus, so this observation is not surprising. Due to this decrease, the WWTP at Nieuwveer would be able to discharge its

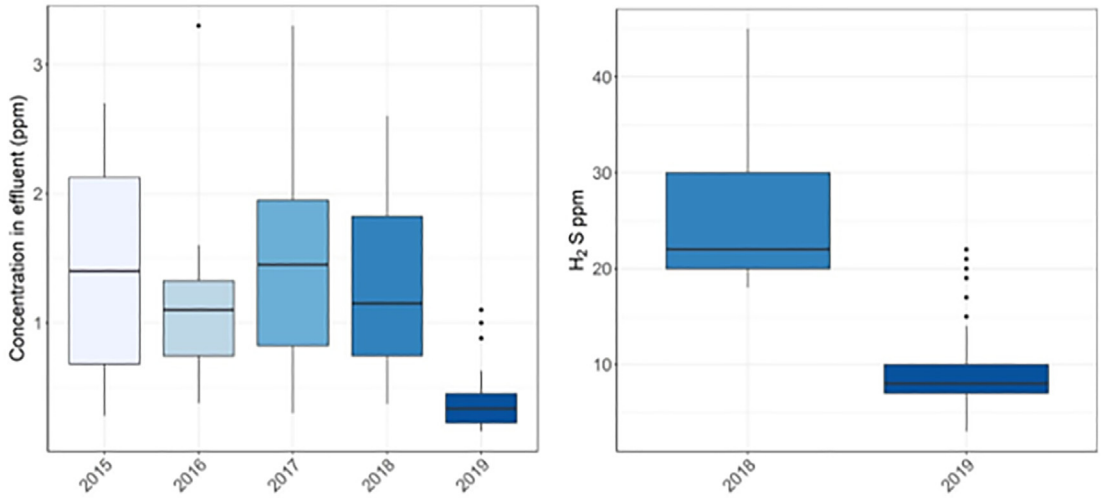

Fig. 6. Data for the Nieuwveer WWTP comparing the time with standard Fe dosing (2015–2018) to the time with doubled Fe dosing (2019) in the period January–April. Left: Phosphorus in the effluent. Right: H_2S in the biogas (the detector's position was changed in 2017 so comparison is only possible for 2018 and 2019).

effluent in a more sensitive body of water closer to the plant, and to improve water availability for agriculture in the region. High Fe dosing and subsequent recovery of phosphorus through vivianite is, therefore, a promising technology for areas where strict effluent limits are applied, such as in countries bordering the Baltic Sea where stringent requirements for effluent P concentration can only be achieved by metal salt dosing (Suresh Kumar et al., 2019).

The quantity of H_2S in the biogas was reduced in Nieuwveer to an average of 8 ppm under higher Fe dosing compared to 26 ppm under normal Fe dosing (Fig. 6). This is in accordance with the observation that Fe can be used to reduce the H_2S in the biogas by binding it as FeS_x (Gutierrez et al., 2010; Mamais et al., 1994). Despite a clear decrease of H_2S in the biogas, an increase of S in the solid fraction of the DS is not noticeable. A mass balance of the S in the digester showed that this H_2S reduction in the biogas corresponds to only 246 g of S per day. It represents 0.08% of the daily S load in the DS, explaining why an increase in the solid S was not noticeable in our measurements (Appendix D). As discussed above, FeS_x forms preferentially over vivianite, so we expected the soluble S pool to be already depleted before the increased Fe dosing. The observed H_2S decrease goes against this thought, but can be explained by thermodynamic: as more Fe is dosed, there is more soluble Fe in the DS. Thus, soluble S is decreasing to keep the solid-liquid equilibrium for $FeS_{x(s)}$ (confirmed by ICP-OES in Appendix D). The chemical potential theory says that the liquid and the gas phase need to be in equilibrium, which can only be matched if S in the gas phase (H_2S) decreases as well.

The data showed no significant change in the nitrogen removal performance of the WWTP after the increased iron dosing (Table 1). In addition, no change in NH_3 removal was observed. This does not necessarily mean that the increased Fe dosing has not affected the nitrogen cycle. Some possible impact of Fe dosing are:

- Higher Fe dosing could improve flocculation in the A-stage, allowing less COD to go to the B-stage, impairing the Nitrogen removal if not enough COD is present to perform denitrification.
- Excessive Fe dosing could also have the opposite effect by destabilizing the flocs, allowing more COD to go to the B-stage and, thus, improving denitrification. According to Bratby et al., (2016), a concentration of Fe^{2+} in the range 0.8–80 ppm allows good flocculation. Our measurements indicate values in this range (10–20 ppm) in the A-stage, indicating that destabilization of the flocs is unlikely.
- Another point to consider is that 10–25% of the nitrogen is organically bound, and will be flocculated in the A-stage as well (Henze et al., 2008), reducing the required COD in the B-stage.

In short, the nitrogen cycle could be affected in several contradictory ways by Fe dosing, not leading to any significant difference. More detailed measurements would be necessary to obtain a clearer answer, but this was not the main objective of the current study.

During increased Fe dosing, COD removal was slightly improved from 91.7% to 93.0% (Table 1). The Fe^{2+} dosed is oxidized in the A-stage to remove COD as is commonly the case. However, 20–50% of the Fe that arrives at the B-stage is still Fe^{2+} and this suggests that the oxidation of the Fe(II) in the A-stage is not optimal (Appendix D). Fe^{2+} is a less strong coagulant than Fe^{3+} due to its lower

Table 1
Integral parameter of the WWTP Nieuwveer with standard Fe dosing and increased Fe dosing. The values presented are the average of the period January to April for year 2015–2018 (standard Fe dosing) and 2019 (increased Fe dosing). Detailed comparison are presented in Appendix J for COD removal, N removal, Biogas production and dewaterability.

Integral parameter	Unit	With standard Fe dosing	With increased Fe dosing
P in effluent	Ppm	1.28	0.42
H_2S in biogas	Ppm	26	8
COD removal	%	91.7	93
N removal	%	71.2	74
Biogas production	m^3/kg dry solid	442	418
Dewaterability	kg PE/g of TS	21.6	21.8

charge. Improved COD removal could still be possible if Fe^{3+} were used in the A-stage or the oxidation of the Fe^{2+} was improved. The water authority Brabantse Delta doses Fe^{2+} salts in Nieuwveer because it is cheaper and not to promote vivianite formation.

The higher Fe dosing did not have a significant impact on biogas production (Table 1). No increase of A sludge production nor COD removal (~50%) in the A-stage was noticed despite more Fe dosed, explaining why the biogas production did not increase. Moreover, the Fe content jumped from 40 mg/g of TS for the 2015–2018 period (considered equal to the 04/12/2018 measurement) to an average of 65 mg/g for 2019 (Fig. 2). This increase reduces the "digestible" content per tons of dry solid by 2–3%, contributing to less biogas production per dry weight of sludge.

Because the dewatered digested sludge is transported before incineration, the sludge volume needs to be minimized to reduce transportation costs. According to the results in Table 1, increased Fe dosing had no measurable effect on the dewaterability of the digested sludge. The percentage of dry matter after dewatering of the digested sludge is comparable to other years, and the same quantity of polymer was used to achieve this dry matter content. However, no specific actions was taken to optimize the sludge dewatering during this test. Higher Fe dosing slightly decreases the VSS in the sludge as it will increase the inorganic content of the sludge (more vivianite formed). The magnetic extraction of the formed vivianite reduces the inorganic content, leading to higher VSS fraction, thus an increased heating value of the sludge after dewatering.

In short, higher Fe dosing did not appear to have any negative impact on the functioning of the WWTP in terms of N removal, dewaterability, biogas production and COD removal (the latter showing slight improvement). On the contrary, it considerably reduced the P level in the effluent and the H_2S content in the biogas.

3.4. Future perspectives for P recovery by magnetic extraction of vivianite

The magnetic extraction of vivianite from DS is possible (Prot et al., 2019), and pilot plant tests for magnetic recovery were taking place in parallel to this study. This study confirmed that increasing Fe dosing increases the share of P as vivianite and, thus, the share of recoverable phosphorus. According to Wilfert et al., (2018), neither the type of Fe salt used nor the type of installation influences the quantity of P present as vivianite after digestion, suggesting that dosing will mainly depend on local aspects and a uniform guideline for practical implementation of higher Fe dosing need not be given. The quantity of Fe dosed should be adapted to the objective of the water authority in terms of P level in the effluent, H2S control and vivianite production. WWTPs seeking to maximize recovery of P as vivianite could aim at a S-corrected Fe/P ratio (see 3.2.2) in the digested sludge higher than 1.5 to convert more than 80% of the P into vivianite.

The cost increase associated with higher Fe dosing is not negligible but can be offset by the savings in sludge disposal and better effluent quality, for example. In the case of Nieuwveer, the increase in Fe dosing was on average 366 kg Fe/day, corresponding to a cost of €304/day (based on a cost price of €0.83/kg for $FeSO_4*7H_2O$ as paid by the WWTP). This WWTP produces 15 tons of dry solids per day with a disposal cost of around €277 per ton of dry solids (assuming 23% dry matter) leading to a daily cost of €4155 (SNB annual report 2018). Assuming that all the extra vivianite formed would be removed from the digested sludge, the amount of dry solid would be reduced by 10%, making a saving of €415/day. Moreover, the oxygen required to oxidize the extra Fe^{2+} dosed in the A-stage represents only 0.1% of the aeration necessary to treat the COD in Nieuwveer. As a result, no extra aeration costs are to be expected (Appendix K).

In the case of WWTP Nieuwveer ca. 90% of the P present in the influent ended up in the sewage sludge at the higher iron dosage. These influent (5 ppm) and effluent (0.5 ppm) values are typical for sewage treatment plants in Northern Europe (Pons et al., 2004). The results of this study and of Wilfert et al., (2018) indicate that if the iron dosage is adjusted to have a Fe/P molar ratio in digested sludge above 1.5, more than 80% of the phosphorus present in digested sludge can be present as vivianite. Our work on pilot scale magnetic separation of vivianite at Nieuwveer revealed that 70–80% of the vivianite in digested sludge could be recovered (unpublished results). Therefore, we expect that stimulation of vivianite formation in combination with magnetic recovery from the sludge could recover 50–60% of the P present in the influent of the Nieuwveer sewage treatment plant. We believe that these results can be extrapolated for all WWTPs bearing an anaerobic digester.

In the future, vivianite recovery could be integrated with dissolution of the vivianite by alkaline treatment (proof of principle in Prot et al., 2019) to recover the phosphorus in any desired form and to enable the reuse of the Fe in the next cycle of phosphate recovery at the WWTP. Vivianite recovery recovers not only the dosed iron but also any iron that was present in the influent wastewater. This makes vivianite recovery of particular interest for WWTPs treating high-Fe bearing industrial wastewater in areas with significant aerobic groundwater intrusion in the sewer network. In countries with strict effluent criteria, the Fe dosage is already high (Fe/P ratio >1.5 is common). Therefore, the digested sludge from these types of plants is often suitable for direct vivianite recovery without additional Fe dosing.

In addition to recovery of P and Fe via an alkaline treatment, vivianite could be used as Fe-fertilizer for Fe-poor soils (Rombolà et al., 2007). Several high-value applications of vivianite could also be considered depending on its purity after separation. Using vivianite as a component in lithium-ion batteries or to create pigments are two such high-value possibilities (Recham et al., 2009, Čermáková et al., 2013).

4. Conclusion

The share of P present as vivianite in digested sludge could be increased from 20% to 50% by dosing more iron in the Nieuwveer WWTP, confirming our earlier hypothesis that a high iron content in the sludge has a direct relation to a higher vivianite content (Wilfert et al., 2018). More importantly all the additional iron that was dosed was used to produce vivianite quickly. This is an important finding as it suggests a way to efficiently increase P recovery potential via vivianite, for instance via magnetic separation from digested sludge. Our analyses suggest that different types of vivianite mineral coexist in digested sludge. Further studies need to be carried out to characterize these minerals, as they could have implications for recovery methods for the vivianite (for instance they may influence the magnetic properties of vivianite) and possible uses of the recovered vivianite.

A thorough study of the WWTP global parameters revealed that the increased Fe dosing did not affect the functioning of the WWTP. Moreover, it effectively reduced the concentration of H_2S in the biogas from 26 to 8 ppm, and more importantly reduced the P in the effluent of the WWTP from 1.3 ppm to 0.4 ppm. This indicates that, especially if very low effluent phosphate is required, a combination of high Fe dosing with vivianite recovery is a promising solution to recover phosphorus from DS.

Declaration of competing interest

The authors declare that they have no known competing financial interests or personal relationships that could have appeared to influence the work reported in this paper.

Acknowledgments

This work was performed in the TTIW-cooperation framework of Wetsus, European Centre of Excellence for Sustainable Water Technology (www.wetsus.nl). Wetsus is funded by the Dutch Ministry of Economic Affairs, the European Union Regional Development Fund, the Province of Fryslân, the City of Leeuwarden and the EZ/Kompas program of the "Samenwerkingsverband Noord-Nederland". We thank the participants of the research theme "Phosphate Recovery" for their financial support and helpful discussions. A special thanks goes to Peter from Brabantse Delta and Gustas who were a great help during the sampling. Additionally, we thank Leonie Hartog for providing valuable information about the treatment parameters of Nieuwveer. We also want to express our gratitude to Pieter van Veelen and Rebeca Pallarès Vega for their precious help with the statistical data analysis. Finally, we want to show appreciation for the input of Philipp Wilfert in the design of this project, and his availability to discuss the results.

Appendix A

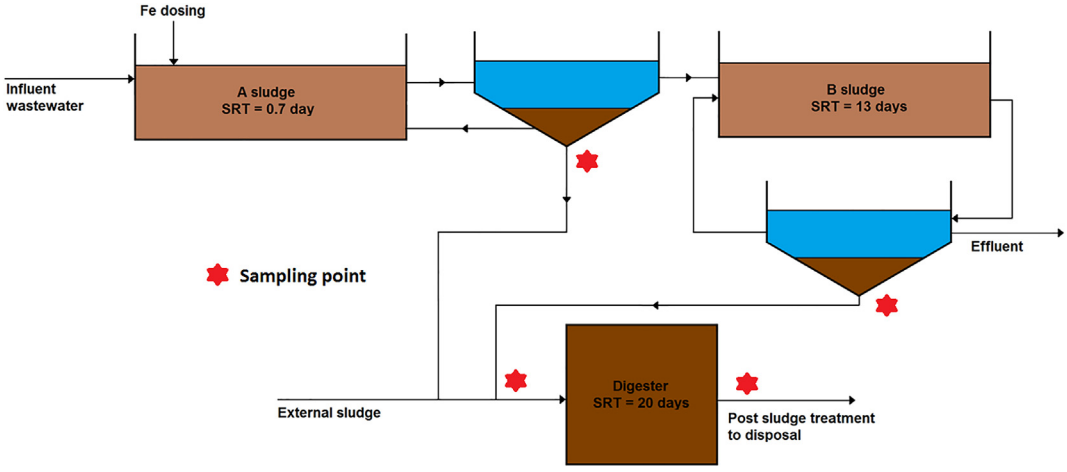

Fig. A1. Simplified flowchart of the WWTP Nieuwveer and sampling points

Table A1
Sampling dates of the WWTP Nieuwveer and corresponding Fe dosing phase

Sample	1	2	3	4	5	6	7	8	9	10	11
Dosing phase	I	I	II	II	II	II	II	II	II	II	III
Date	04/12 2018	19/12 2018	08/01 2019	22/01 2019	05/02 2019	19/02 2019	12/03 2019	02/04 2019	16/04 2019	30/04 2019	28/05 2019

Appendix B

Table B1
Mössbauer results for all solid samples from Nieuwveer studied. (DS = digested sludge, MS = mixed sludge, A = A-stage sludge, B=B-stage sludge). Fe^{3+}/Fe^{II}: Fe^{3+} species other than vivianite and low-spin Fe^{2+} compounds like pyrite. Fe^{3+} (Viv. A + B): total Fe^{3+} vivianite. Fe^{2+} (Viv. A): Fe^{2+} in the site A of vivianite. Fe^{2+} (Viv. B): Fe^{2+} in the site B of vivianite.

Sample	Isomer Shift ($mm \cdot s^{-1}$)	Quadrupole Splitting ($mm \cdot s^{-1}$)	Γ ($mm \cdot s^{-1}$)	Phase	Spectral contribution (%)
Synthetic vivianite	0.46	0.63	0.52	Fe^{3+} (Viv. A + B)	46
	1.17	2.48	0.37	Fe^{2+} (Viv. A)	18
	1.22	2.99	0.37	Fe^{2+} (Viv. B)	36
DS1	0.31	0.82	0.55	Fe^{3+}/Fe^{II}	59
	0.46	0.63	0.52	Fe^{3+} (Viv. A + B)	13
	1.23	2.35	0.32	Fe^{2+} (Viv. A)	16
	1.22	3.05	0.32	Fe^{2+} (Viv. B)	12
DS2	0.31	0.64	0.66	Fe^{3+}/Fe^{II}	41
	0.46	0.63	0.52	Fe^{3+} (Viv. A + B)	19
	1.22	2.43	0.33	Fe^{2+} (Viv. A)	18
	1.25	2.97	0.33	Fe^{2+} (Viv. B)	22
DS3	0.31	0.41	0.62	Fe^{3+}/Fe^{II}	54
	0.46	0.63	0.52	Fe^{3+} (Viv. A + B)	12
	1.21	2.43	0.30	Fe^{2+} (Viv. A)	18
	1.26	2.92	0.30	Fe^{2+} (Viv. B)	16
DS4	0.31	0.83	0.57	Fe^{3+}/Fe^{II}	31
	0.46	0.63	0.52	Fe^{3+} (Viv. A + B)	23
	1.22	2.42	0.33	Fe^{2+} (Viv. A)	20
	1.24	2.97	0.33	Fe^{2+} (Viv. B)	26
DS5	0.31	0.56	0.72	Fe^{3+}/Fe^{II}	34
	0.46	0.63	0.52	Fe^{3+} (Viv. A + B)	24
	1.20	2.45	0.32	Fe^{2+} (Viv. A)	17
	1.25	2.97	0.32	Fe^{2+} (Viv. B)	25
DS6	0.31	0.89	0.53	Fe^{3+}/Fe^{II}	25
	0.46	0.63	0.52	Fe^{3+} (Viv. A + B)	26
	1.21	2.42	0.34	Fe^{2+} (Viv. A)	21
	1.24	2.96	0.34	Fe^{2+} (Viv. B)	28
DS7	0.31	0.86	0.56	Fe^{3+}/Fe^{II}	28
	0.46	0.63	0.52	Fe^{3+} (Viv. A + B)	24
	1.22	2.41	0.34	Fe^{2+} (Viv. A)	19
	1.24	2.95	0.34	Fe^{2+} (Viv. B)	29
DS8	0.31	0.89	0.59	Fe^{3+}/Fe^{II}	32
	0.46	0.63	0.52	Fe^{3+} (Viv. A + B)	23
	1.23	2.43	0.33	Fe^{2+} (Viv. A)	19
	1.25	2.97	0.33	Fe^{2+} (Viv. B)	26
DS9	0.31	0.85	0.57	Fe^{3+}/Fe^{II}	24
	0.46	0.63	0.52	Fe^{3+} (Viv. A + B)	23
	1.20	2.42	0.33	Fe^{2+} (Viv. A)	22
	1.23	2.92	0.33	Fe^{2+} (Viv. B)	31
DS10	0.31	0.80	0.55	Fe^{3+}/Fe^{II}	26
	0.46	0.63	0.52	Fe^{3+} (Viv. A + B)	21
	1.20	2.41	0.35	Fe^{2+} (Viv. A)	22
	1.23	2.93	0.35	Fe^{2+} (Viv. B)	31
DS11	0.31	0.86	0.59	Fe^{3+}/Fe^{II}	59
	0.46	0.63	0.52	Fe^{3+} (Viv. A + B)	13
	1.23	2.34	0.34	Fe^{2+} (Viv. A)	15
	1.26	2.93	0.34	Fe^{2+} (Viv. B)	14
MS2	0.31	0.61	0.67	Fe^{3+}/Fe^{II}	51
	0.46	0.63	0.52	Fe^{3+} (Viv. A + B)	16
	1.24	2.40	0.31	Fe^{2+} (Viv. A)	14
	1.26	2.92	0.31	Fe^{2+} (Viv. B)	19
MS6	0.31	0.41	0.59	Fe^{3+}/Fe^{II}	76
	0.46	0.63	0.52	Fe^{3+} (Viv. A + B)	8
	1.24	2.33	0.34	Fe^{2+} (Viv. A)	7
	1.26	2.89	0.34	Fe^{2+} (Viv. B)	9
A11	0.34	0.60	0.64	Fe^{3+}/Fe^{II}	84
	1.35	2.57	0.40	Fe^{2+}	16
B11	0.31	0.65	0.68	Fe^{3+}/Fe^{II}	72
	1.20	2.21	0.40	Fe^{2+} (Viv. A)	9
	1.25	2.82	0.40	Fe^{2+} (Viv. B)	19

In the following Mössbauer spectra the colored curves represent the following:

- Black: total spectrum
- Red: Fe^{2+} in vivianite site I
- Blue: Fe^{2+} in vivianite site II
- Pink: Fe^{3+} in vivianite I + II
- Green: Fe^{3+}/Fe^{II} for Fe^{3+} compound excluding vivianite and low-spin Fe^{2+} like pyrite

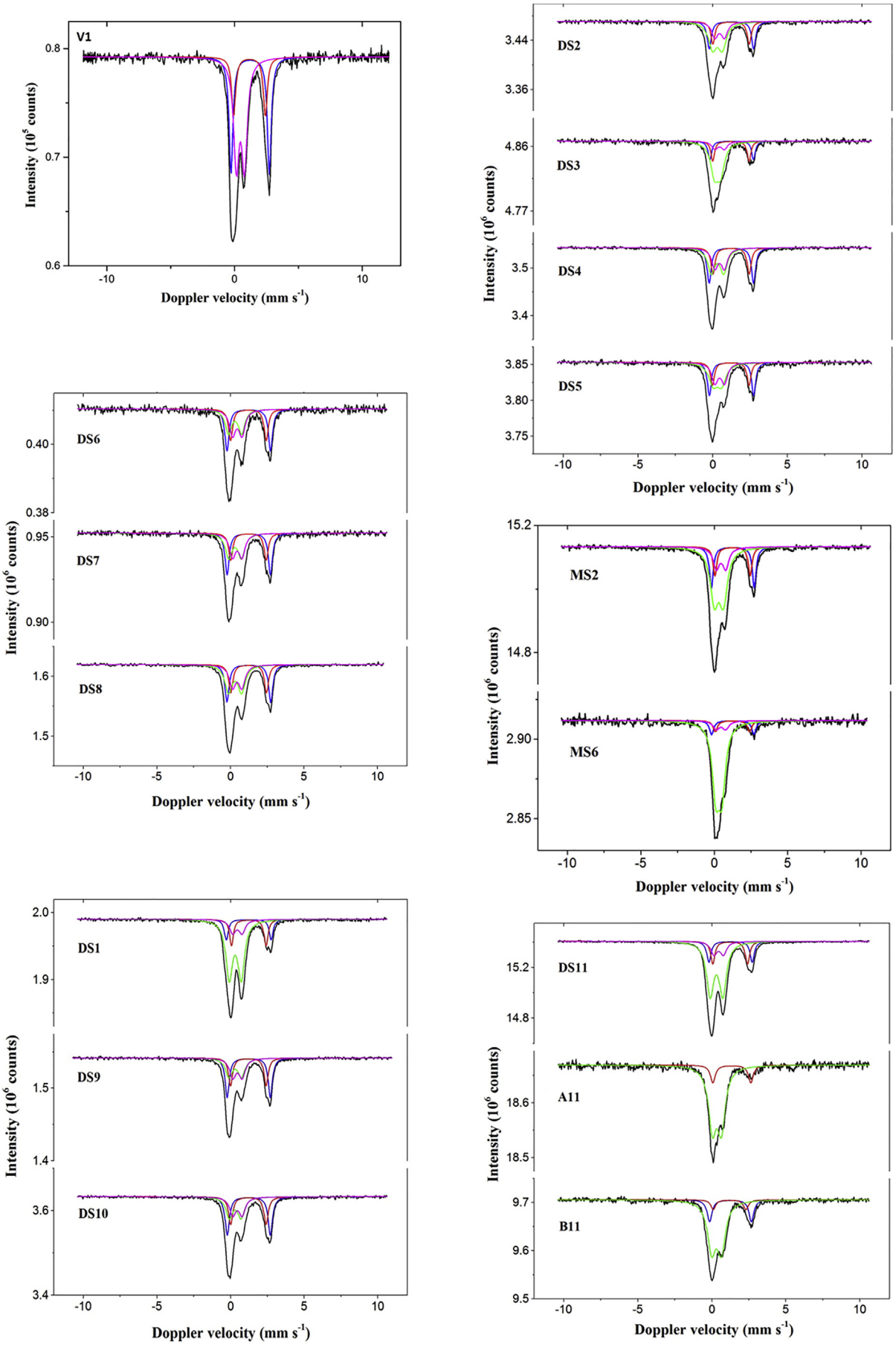

Fig. B1. Mössbauer spectra for all the DS samples, synthetic vivianite (V1), A11, B11, MS2 and MS6

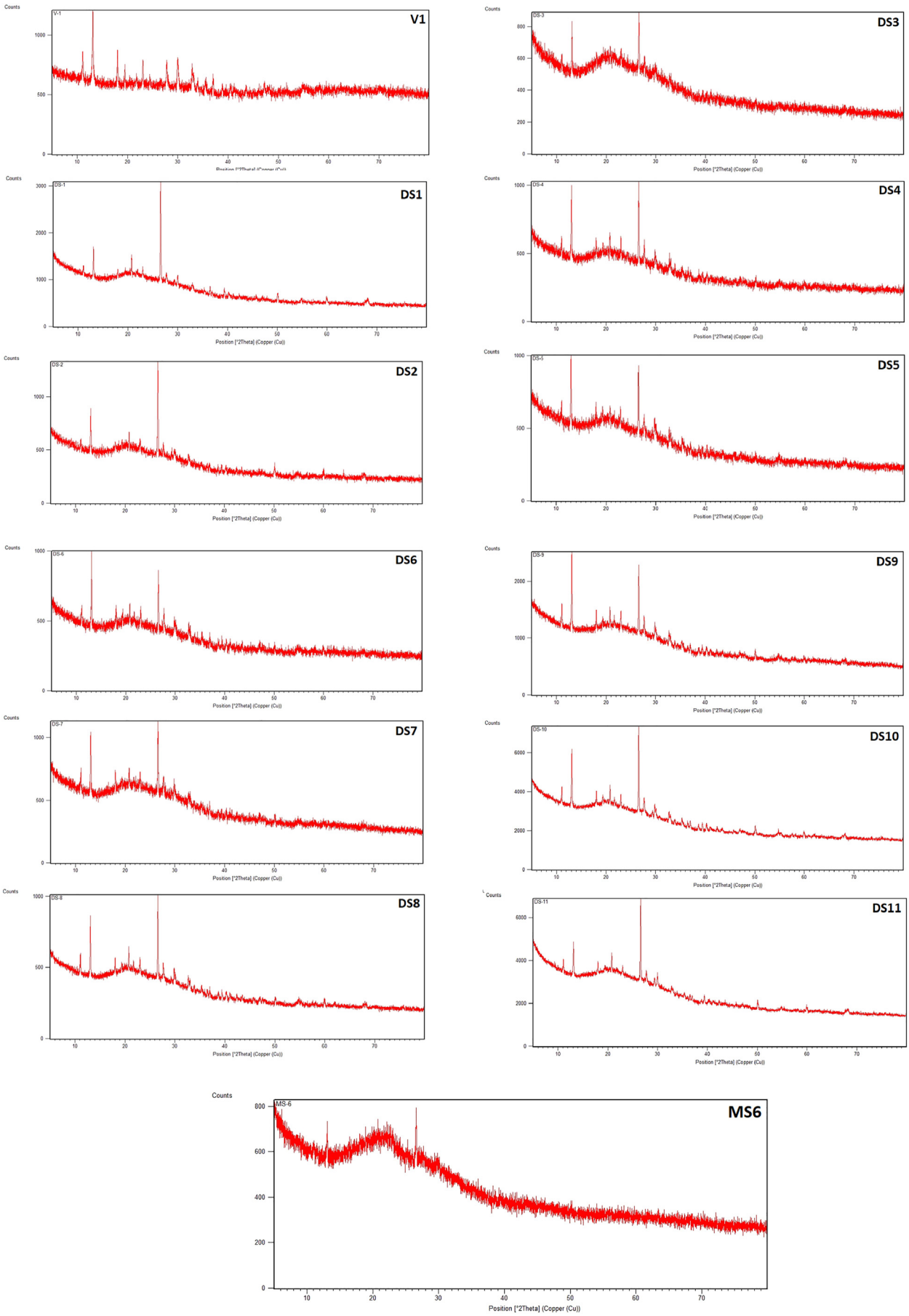

Fig. C1. XRD spectra for all the DS samples, synthetic vivianite (V1) and MS6

Appendix C

Appendix D

Table D1
Solid composition of the sludge A, B and digested measured by ICP-OES

Sludge sample		Fe (mg/g TS)	P (mg/g TS)	S (mg/g TS)	Ca (mg/g TS)	Mg (mg/g TS)
4-12-2018	DS1	40,50 ± 1.16	30,96 ± 0.66	12,49 ± 0.38	28,56 ± 0.47	3,49 ± 0.09
19-12-2018	DS2	46,38 ± 0.43	31,95 ± 0.67	11,60 ± 0.30	26,72 ± 0.69	3,54 ± 0.05
8-1-2019	DS3	53,28 ± 1.73	34,18 ± 0.14	10,48 ± 0.37	25,58 ± 1.06	3,85 ± 0.09
22-1-2019	DS4	61,54 ± 1.80	36,88 ± 0.65	11,06 ± 0.04	28,18 ± 0.13	3,57 ± 0.07
5-2-2019	DS5	58,87 ± 0.71	32,47 ± 0.33	10,65 ± 0.05	25,40 ± 0.11	2,95 ± 0.03
19-2-2019	DS6	63,94 ± 2.18	34,47 ± 0.74	10,63 ± 0.11	26,70 ± 0.37	3,10 ± 0.08
12-3-2019	DS7	63,23 ± 1.24	36,65 ± 0.49	10,66 ± 0.07	24,67 ± 0.20	2,96 ± 0.05
2-4-2019	DS8	68,51 ± 0.64	35,59 ± 0.16	10,19 ± 0.29	23,71 ± 0.74	3,07 ± 0.02
16-4-2019	DS9	71,13 ± 1.69	36,48 ± 0.67	10,49 ± 0.03	26,78 ± 0.35	3,17 ± 0.03
30-4-2019	DS10	67,44 ± 0.85	36,14 ± 0.47	11,37 ± 0.08	28,37 ± 0.12	3,24 ± 0.02
28-5-2019	DS11	55,95 ± 1.02	35,17 ± 0.70	13,90 ± 0.52	30,93 ± 0.52	3,55 ± 0.06
4-12-2018	A1	22,04 ± 0.05	15,92 ± 0.01	7,38 ± 0.20	19,44 ± 0.14	2,26 ± 0.02
19-12-2018	A2	37,71 ± 0.88	22,05 ± 0.55	7,58 ± 0.23	18,79 ± 0.44	1,81 ± 0.04
8-1-2019	A3	34,30 ± 0.30	17,82 ± 0.14	6,26 ± 0.13	15,75 ± 0.15	1,31 ± 0.01
22-1-2019	A4	60,68 ± 0.34	27,16 ± 0.24	7,05 ± 0.05	19,66 ± 0.23	1,74 ± 0.02
5-2-2019	A5	48,84 ± 1.57	21,61 ± 0.41	6,45 ± 0.18	15,06 ± 0.48	1,42 ± 0.02
19-2-2019	A6	51,37 ± 1.27	24,53 ± 0.38	7,12 ± 0.08	16,58 ± 0.33	1,70 ± 0.01
12-3-2019	A7	41,07 ± 1.48	18,69 ± 0.62	6,44 ± 0.03	11,48 ± 0.21	1,40 ± 0.01
2-4-2019	A8	33,72 ± 0.27	19,06 ± 0.10	9,01 ± 0.03	17,60 ± 0.15	1,70 ± 0.01
16-4-2019	A9	45,96 ± 0.81	22,55 ± 0.14	7,28 ± 0.07	18,96 ± 0.29	1,62 ± 0.01
30-4-2019	A10	30,27 ± 0.26	16,93 ± 0.09	10,67 ± 0.10	17,03 ± 0.14	1,68 ± 0.02
28-5-2019	A11	24,78 ± 0.28	15,29 ± 0.19	11,38 ± 0.08	19,84 ± 0.22	1,67 ± 0.01
4-12-2018	B1	28,06 ± 0.64	26,44 ± 0.59	8,79 ± 0.21	19,52 ± 0.29	3,47 ± 0.06
19-12-2018	B2	28,81 ± 0.41	24,31 ± 0.33	7,56 ± 0.09	15,83 ± 0.23	2,60 ± 0.04
8-1-2019	B3	31,88 ± 0.43	24,45 ± 0.34	7,50 ± 0.10	16,82 ± 0.13	2,34 ± 0.03
22-1-2019	B4	35,60 ± 0.19	24,53 ± 0.19	7,89 ± 0.08	16,20 ± 0.15	2,42 ± 0.01
5-2-2019	B5	32,82 ± 0.73	21,79 ± 0.40	7,51 ± 0.06	13,39 ± 0.27	2,03 ± 0.04
19-2-2019	B6	38,41 ± 1.48	22,75 ± 0.79	7,67 ± 0.23	14,56 ± 0.55	2,19 ± 0.08
12-3-2019	B7	37,39 ± 0.15	22,07 ± 0.08	7,11 ± 0.05	13,49 ± 0.07	2,02 ± 0.01
2-4-2019	B8	43,86 ± 0.83	24,47 ± 0.55	6,76 ± 0.13	17,26 ± 0.29	2,49 ± 0.05
16-4-2019	B9	34,17 ± 0.99	23,56 ± 0.62	8,00 ± 0.15	16,15 ± 0.42	2,49 ± 0.07
30-4-2019	B10	41,91 ± 0.22	27,58 ± 0.16	7,79 ± 0.06	17,99 ± 0.11	2,46 ± 0.01
28-5-2019	B11	39,88 ± 0.27	30,20 ± 0.21	7,90 ± 0.06	22,66 ± 0.09	2,58 ± 0.02

Table D2
pH of the A, B, MS and digested sludge sample of Nieuwveer

Date	A	B	DS	MS
4-12-2018	5,91 ± 0.01	6,48 ± 0.01	7,48 ± 0.01	ND
19-12-2018	6,52 ± 0.03	6,87 ± 0.02	7,48 ± 0.04	5,03 ± 0.01
8-1-2019	6,45 ± 0.09	6,93 ± 0.02	7,69 ± 0.03	5,19 ± 0.01
22-1-2019	6,85 ± 0.06	6,95 ± 0.08	8,14 ± 0.01	3,69 ± 0.01
5-2-2019	6,86 ± 0.07	7,11 ± 0.04	8,19 ± 0.01	4,62 ± 0.01
19-2-2019	6,59 ± 0.04	6,84 ± 0.01	7,76 ± 0.06	3,94 ± 0.01
12-3-2019	8,20 ± 0.01	8,22 ± 0.01	8,45 ± 0.01	4,56 ± 0.01
2-4-2019	6,51 ± 0.01	6,97 ± 0.02	8,52 ± 0.07	5,05 ± 0.01
16-4-2019	7,09 ± 0.08	7,53 ± 0.01	8,30 ± 0.01	3,93 ± 0.01
30-4-2019	6,17 ± 0.11	6,78 ± 0.04	8,02 ± 0.01	4,38 ± 0.01
28-5-2019	6,31 ± 0.01	7,26 ± 0.04	8,16 ± 0.02	4,65 ± 0.01

Table D3
Solid content (%) of the sludge sample of Nieuwveer

Date	A	B	DS	MS
4-12-2018	1,08 ± 0.02	0,81 ± 0.01	4,69 ± 0.01	12,89 ± 0.06
19-12-2018	0,74 ± 0.01	0,55 ± 0.01	3,95 ± 0.08	9,15 ± 0.01
8-1-2019	1,00 ± 0.01	0,63 ± 0.02	4,01 ± 0.01	7,50 ± 0.05
22-1-2019	0,68 ± 0.02	0,64 ± 0.01	4,00 ± 0.01	2,89 ± 0.04
5-2-2019	0,90 ± 0.01	0,70 ± 0.01	3,69 ± 0.08	1,32 ± 0.02
19-2-2019	0,59 ± 0.02	0,53 ± 0.03	4,42 ± 0.04	0,77 ± 0.02
12-3-2019	1,14 ± 0.02	0,75 ± 0.01	3,68 ± 0.01	3,36 ± 0.01
2-4-2019	1,13 ± 0.01	0,59 ± 0.01	4,07 ± 0.03	2,60 ± 0.06
16-4-2019	0,59 ± 0.01	0,40 ± 0.01	4,31 ± 0.03	0,98 ± 0.01
30-4-2019	0,66 ± 0.05	0,60 ± 0.03	4,25 ± 0.09	0,93 ± 0.01
28-5-2019	0,86 ± 0.06	0,37 ± 0.01	4,04 ± 0.11	1,53 ± 0.01

Table D4
Iron speciation in sludge A, B and digested in Nieuwveer obtained by the ferrozine method

Sample	Fe^{2+} (ppm)	Fe^{3+} (ppm)	Total Fe (ppm)
A1	9,60 ± 0.02	1,07 ± 0.10	10,67 ± 0.08
A2	12,08 ± 0.19	−0,56 ± 0.64	11,52 ± 0.45
A3	10,17 ± 0.32	2,84 ± 0.73	13,01 ± 0.41
A4	12,02 ± 0.32	1,16 ± 0.18	13,18 ± 0.50
A5	14,57 ± 0.13	2,13 ± 0.06	16,69 ± 0.07
A6	14,07 ± 0.37	3,14 ± 0.70	17,21 ± 0.52
A7	49,31 ± 2.47	8,49 ± 0.42	57,79 ± 2.89
A8	16,50 ± 0.06	3,02 ± 0.37	17,66 ± 0.43
A9	5,83 ± 0.03	2,97 ± 0.32	7,90 ± 0.35
A10	12,14 ± 0.60	1,97 ± 0.33	14,11 ± 0.27
A11	14,11 ± 0.13	4,73 ± 0.02	18,84 ± 0.16
B1	3,03 ± 1.12	0,35 ± 0.02	3,38 ± 1.14
B2	0,11 ± 0.06	0,10 ± 0.03	0,21 ± 0.03
B3	0,20 ± 0.01	0,09 ± 0.05	0,29 ± 0.05
B4	0,12 ± 0.01	0,89 ± 0.07	1,01 ± 0.08
B5	0,70 ± 0.16	0,30 ± 0.04	1,00 ± 0.20
B6	0,14 ± 0.02	0,62 ± 0.04	0,76 ± 0.05
B7	1,45 ± 0.01	0,95 ± 0.08	2,40 ± 0.07
B8	0,11 ± 0.01	0,60 ± 0.01	0,49 ± 0.01
B9	0,11 ± 0.01	0,37 ± 0.01	0,38 ± 0.01
B10	0,14 ± 0.01	0,24 ± 0.09	0,38 ± 0.09
B11	0,10 ± 0.01	0,46 ± 0.06	0,56 ± 0.06
DS1	0,47 ± 0.05	5,41 ± 0.35	5,88 ± 0.30
DS2	0,62 ± 0.01	10,70 ± 0.31	11,32 ± 0.32
DS3	0,07 ± 0.02	10,57 ± 1.26	10,63 ± 1.28
DS4	0,85 ± 0.12	21,57 ± 2.10	22,43 ± 2.23
DS5	0,91 ± 0.28	22,25 ± 8.61	23,16 ± 8.89
DS6	1,89 ± 0.01	41,95 ± 0.13	43,84 ± 0.12
DS7	46,63 ± 0.36	15,53 ± 2.07	62,16 ± 1.72
DS8	40,22 ± 0.01	11,57 ± 1.32	50,51 ± 1.33
DS9	1,24 ± 0.02	24,38 ± 0.15	28,07 ± 0.17
DS10	1,14 ± 0.02	29,83 ± 0.09	30,98 ± 0.07
DS11	0,52 ± 0.01	22,90 ± 0.24	23,42 ± 0.23

Appendix E

Thermodynamic evaluations were carried out with Visual Minteq to study the stable minerals that could form in the digested sludge under the pH and concentrations conditions in the Nieuwveer WWTP. The saturation index, as defined in Mersmann, 2001, indicates how thermodynamically favored a precipitation reaction is. For vivianite, its expression is:

$$SI = \log\left(\frac{IAP}{K_s}\right)$$

with

$$IAP = (\gamma_{Fe^{2+}} * C_{Fe^{2+}})^3 (\gamma_{PO_4^{3-}} * C_{PO_4^{3-}})^2$$

Where:

- SI is the saturation index
- K_s is the solubility product of vivianite at 25 °C worth $10^{-35.76}$ (Al-Borno and Tomson, 1994)
- γ is the activity coefficient of the ion in solution in mol/L
- C the concentration of the ion in solution in mol/L

With this definition, a solid can theoretically form if its SI is > 0. The higher the SI, the higher the chances of formation. Vivianite always presents a SI > 0, which confirms that its formation is thermodynamically possible. Its SI values are mainly comprised between 2 and 5, suggesting that it is the equilibrium zone for vivianite in digested sludge. Some discrepancies concerning the value of the pKs of vivianite can be found in literature. While most of the researchers suggest a pKs value around 35–37 (Al-Borno and

Table D5
Liquid fraction composition of the digested sludge obtained by ICP-EOS

DS	Fe (ppm)	P (ppm)	S (ppm)	Ca (ppm)	Mg (ppm)
DS1	5,01	90,79	11,79	65,71	7,75
DS2	13,15 ± 0.66	74,57 ± 3.73	13,38 ± 0.67	75,60 ± 3.78	1,92 ± 0.10
DS3	9,68 ± 0.48	71,13 ± 3.73	8,86 ± 0.44	65,21 ± 3.26	16,53 ± 0.83
DS4	21,47 ± 1.07	39,95 ± 2.00	6,45 ± 0.32	96,88 ± 4.84	22,13 ± 1.11
DS5	43,16 ± 2.16	43,51 ± 2.18	5,93 ± 0.30	130,77 ± 6.54	26,52 ± 1.33
DS6	44,50 ± 2.22	28,43 ± 1.42	9,21 ± 0.46	145,23 ± 7.26	28,63 ± 1.43
DS7	52,40 ± 2.62	50,45 ± 2.52	4,29 ± 0.21	ND	26,08 ± 1.30
DS8	50,21 ± 2.51	56,91 ± 2.85	5,33 ± 0.27	125,92 ± 6.30	28,07 ± 1.40
DS9	28,21 ± 1.41	38,73 ± 1.94	8,41 ± 0.42	107,63 ± 5.38	26,26 ± 1.31
DS10	29,77 ± 1.49	51,91 ± 2.60	9,39 ± 0.47	95,69 ± 4.78	24,62 ± 1.23
DS11	21,32 ± 1.07	87,86 ± 4.39	10,92 ± 0.55	81,89 ± 4.09	25,65 ± 1.28

Table E1
Saturation index for the minerals suspected to be present in digested sludge calculated with Visual Minteq

	SI (vivianite)	SI (struvite)	SI (FeOOH)	SI (strengite)	SI (FeS)	Greigite
DS1	2,43	−0,30	5,93	5,25	−0,34	26,70
DS2	2,83	−0,95	6,27	5,63	−0,20	27,70
DS3	0,42	0,18	6,46	5,20	−0,93	26,40
DS4	4,66	0,59	7,14	5,06	0,56	27,30
DS5	4,59	0,73	8,83	4,76	0,63	27,19
DS6	4,58	0,18	7,09	5,33	0,53	28,68
DS7	10,17	1,01	7,07	4,12	1,80	21,78
DS8	10,14	1,15	6,94	3,93	1,98	22,19
DS9	5,18	0,93	7,23	4,59	0,89	27,78
DS10	4,58	0,78	7,17	5,19	0,57	28,25
DS11	3,85	1,01	7,14	5,12	0,36	27,86

Tomson, 1994; Nriagu, 1972; Rosenqvist, 1970), Liu et al., 2018 proposed a higher value ~40. Hypothesizing this value, the SI in our study would be significantly lower: between −2 and 1. Negative SI seems impossible considering that vivianite is forming in DS, indicating that the pKs given by Liu et al., 2018 may be overestimated. Therefore, we considered the pKs = 35.76 from Al Borno et al. in our modelling.

It is interesting to note that the formation of amorphous FeS is also possible (SI > 0). Another FeS_x compound, greigite ($Fe^{(II)}$-$Fe^{(III)}{}_2S_4$), known to be an amorphous intermediate to the formation of pyrite (Morse et al., 1998), is always saturated with SI values > 25, and its presence cannot be excluded. Numerous Fe oxides including ferrihydrite, magnetite or hematite also have high SI (>7) and could be formed even though no clear evidence of their presence was found. The formation of struvite and strengite ($FePO_4$*$2H_2O$) is also thermodynamically possible according to our simulation, but no trace of these compounds was found by XRD or Mössbauer. Visual Minteq does not take into account some parameters (like kinetics and activation energy) in its model, which can explain the discrepancies between the prediction and reality. For example, it is common that a mineral kinetically favored forms over a mineral thermodynamically favored (Brown et al., 1985).

In short, the SI values obtained in this simulation do not allow to draw clear conclusions but support the presence of FeS_x and the formation of vivianite over less favored P mineral as strengite or struvite.

Table E2
Input data for Minteq modelling. P, Mg^{2+} and S have calculated by ICP-OES. Fe^{2+} and Fe^{2+} have been determined by the ferrozine method. NH_4^+ value is an average of the online measurement realized by the operator of the WWTP on the period of study (Dec. 2018–Apr. 2019). Results of DS7 and DS8 are to be carefully considered as the WWTP Nieuwveer was having some maintenance in those periods.

(ppm)	pH	P	Fe^{2+}	Fe^{3+}	Mg^{2+}	NH_4^+	S
DS1	7.48	90.79	0.47	5.41	7.75	250	11.79
DS2	7.48	74.57	0.62	10.70	1.92	250	13.38
DS3	7.69	71.13	0.07	10.57	16.53	250	8.86
DS4	8.14	39.95	0.85	21.57	22.13	250	6.45
DS5	8.19	43.51	0.91	22.25	26.52	250	5.93
DS6	7.76	28.43	1.89	41.95	28.63	250	9.21
DS7	8.45	50.45	46.63	15.53	26.08	250	4.29
DS8	8.52	56.91	40.22	11.57	28.07	250	5.33
DS9	8.30	38.73	1.24	24.38	26.26	250	8.41
DS10	8.02	51.91	1.14	29.83	24.62	250	9.39
DS11	8.16	87.86	0.52	22.90	25.65	250	10.92

Table F1
Distribution of P, Fe and S in the digested sludge in December 2018 and from January to April 2019 (average values taken)

Period	gaz (kg/day)	Liquid (kg/day)	Solid (kg/day)
P (Dec. 2018)	0,00	32	519
Fe (Dec. 2018)	0,00	3	717
S (Dec. 2018)	0,16	5	199
P (Jan–Apr. 2019)	0,00	19	587
Fe (Jan–Apr. 2019)	0,00	14	1054
S (Jan–Apr. 2019)	0,15	3	177

Table F2
Average daily mass balance for Fe and P for the period with normal Fe dosing (Dec. 2018) and increased Fe dosing (Jan.–Apr. 2019). The sum of the incoming streams (Influent, Dosing and external sludge) is higher that of the discharge streams (effluent and digested sludge) and can be due to an overestimation of the Fe and P in the external sludge (measured once by Wilfert et al., 2018).

kg/day	Fe		P	
	Dec. 2018	Jan.–Apr. 2019	Dec. 2018	Jan.–Apr. 2019
Influent	163	163	598	598
Dosing	555	860	0	0
External sludge	172	172	110	110
Effluent	15	20	73	32
Digested sludge	744	1093	569	620

Table F3
Average concentration of Fe and P in the influent and effluent for the period with normal Fe dosing (Dec. 2018) and increased Fe dosing (Jan.–Apr. 2019)

mg/L	Fe		P	
	Dec. 2018	Jan.–Apr. 2019	Dec. 2018	Jan.–Apr. 2019
Influent	1.9	1.9	7.2	7.85
Effluent	0.18	0.26	0.88	0.42

Appendix F

Table H1
Solid composition (ICP-OES & Mössbauer spectroscopy) of the digested sludge studied by Wilfert et al., (2016) & 2018, and in this study (calculated from Appendix B and Appendix D).

Source	Sample	S (mg/g TS)	Fe (mg/g TS)	P (mg/g TS)	Fe in FeS (mg/g TS)	S-Corrected Fe/P	P in viv. (%)
W. 2015	Lwd	9	40,5	39,4	7,85	0,46	22%
W. 2015	Nieuw.	10,3	57,4	35,8	17,96	0,61	48%
W. 2018	Lwd	6,2	43,4	47,8	10,81	0,38	15%
W. 2018	Berlin	26,4	103,5	35,4	46,04	0,90	85%
W. 2018	Espoo	8,3	134,7	31,7	14,47	2,11	102%
W. 2018	Asten	8,7	11	43,3	15,17	−0,05	0%
W. 2018	Cologne 300K	8,1	100,6	35,5	14,12	1,35	61%
W. 2018	Cologne 100K	8,1	100,6	35,5	14,12	1,35	81%
W. 2018	Cologne 4,2K	8,1	100,6	35,5	14,12	1,35	88%
W. 2018	Dokhaven	11,4	73,9	36,8	19,88	0,82	63%
W. 2018	Nieuw.	8,4	61,6	41,8	14,65	0,62	49%
W. 2018	Espoo 300K	8,3	134,7	31,7	14,47	2,11	82%
W. 2018	Espoo 100K	8,3	134,7	31,7	14,47	2,11	93%
W. 2018	Espoo 4,2K	8,3	134,7	31,7	14,47	2,11	68%
This study	DS1	12,5	40,5	31,0	21,78	0,34	20%
This study	DS2	11,6	46,4	32,0	20,23	0,45	32%
This study	DS3	10,5	53,3	34,2	18,27	0,57	27%
This study	DS4	11,1	61,5	36,9	19,29	0,64	43%
This study	DS5	10,7	58,9	32,5	18,57	0,69	44%
This study	DS6	10,6	63,9	34,5	18,54	0,73	51%
This study	DS7	10,7	63,2	36,7	18,59	0,68	46%
This study	DS8	10,2	68,5	35,6	17,77	0,79	48%
This study	DS9	10,5	71,1	36,5	18,29	0,80	55%
This study	DS10	11,4	67,4	36,1	19,83	0,73	51%
This study	DS11	13,9	56,0	35,2	24,24	0,50	25%

Table I1
Peak height and crystallite size as measured by XRD for the samples of the digested sludge from Nieuwveer

Sample name	Date	Vivianite in DS (mg/g of TS)	Peak position (°2θ)	Peak height (cts)	Crystallite size (Å)
DS 1	4-12-2018	49.7 ± 10.9	11,083	165	1122 ± 30
			13,109	660	
DS 2	19-12-2018	81.9 ± 12.5	11,093	90	1221 ± 223
			13,073	400	
DS 3	8-1-2019	73.4 ± 14.4	11,081	65	1160 ± 233
			13,079	240	
DS 4	22-1-2019	127.1 ± 16.6	11,086	120	1054 ± 69
			13,065	445	
DS 5	5-2-2019	116.3 ± 15.9	11,085	135	1438 ± 101
			13,07	490	
DS 6	19-2-2019	143.6 ± 17.2	11,093	125	1237 ± 166
			13,08	480	
DS 7	12-3-2019	136.3 ± 17.0	11,088	155	1353 ± 123
			13,073	455	
DS 8	2-4-2019	139.5 ± 18.5	11,095	160	1237 ± 131
			13,07	425	
DS 9	16-4-2019	161.9 ± 19.2	11,084	423	1425 ± 46
			13,06	1385	
DS 10	30-4-2019	149.4 ± 18.2	11,087	273	1325 ± 140
			13,062	927	
DS 11	28-5-2019	70.4 ± 15.1	11,094	174	1475
			13,101	524	

Table I2
Concentration of the most present ions in magnetic concentrates produced by our pilot plant in Nieuwveer

g/g of P	Ca	Cu	Mg	Mn	Zn
14-jan	0,157	0000	0,121	0012	0,008
6-feb	0,296	0005	0,098	0012	0,011
8-mar	0,178	0002	0,073	0011	0,007
9-apr	0,218	0003	0,070	0012	0,007
21-may	0,216	0002	0,092	0011	0,005

Table J1
Dewaterability of the digested sludge for the period January–April at the WWTP Nieuwveer (TS stands for Total Solid content of the dewatered sludge and PE stands for PolyElectrolyte: Kemira superfloc C-62089 Cationic)

Year	2015	2016	2017	2018	2019
TS (%)	21,4	22,6	20,2	22,3	21,8
kg PE/g of TS	10,4	10,8	12,1	11,3	10,8

Appendix G

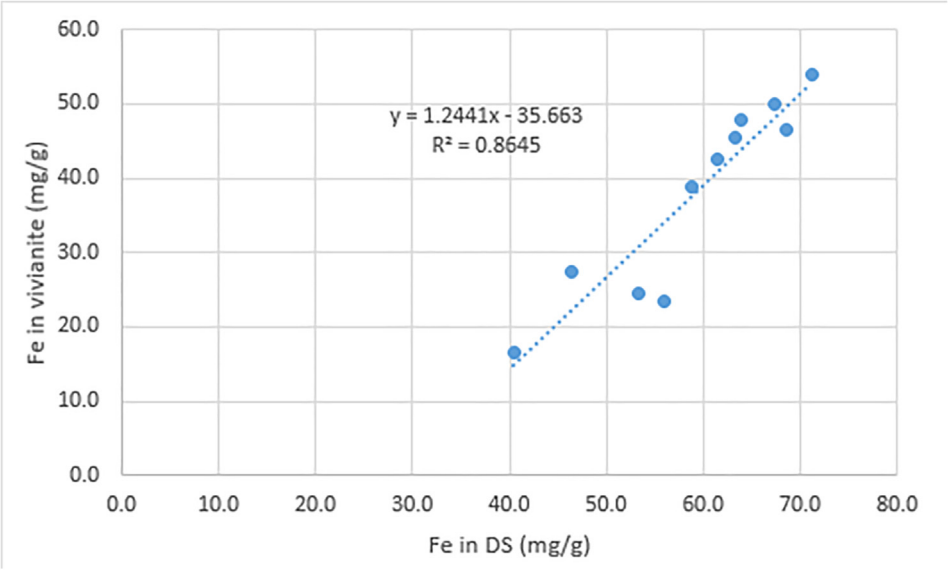

Fig. G1. Iron quantity in vivianite as a function of the iron content in the digested sludge of Nieuwveer (calculated from Appendix D)

The intercept of the regression line with the X-axis suggests that 28 ± 10 mg/g of Fe are needed in sludge before seeing any vivianite formation. This value seems high but has a big deviation, so further interpretation is risky.

Appendix H

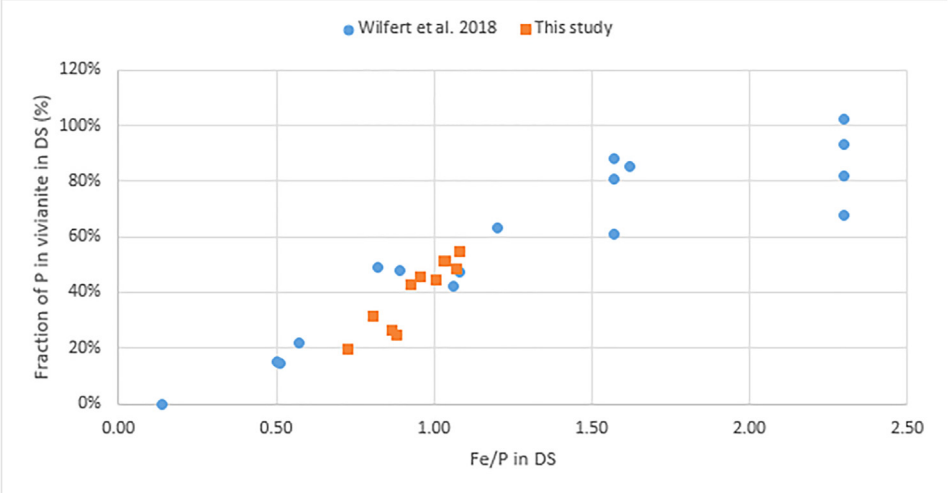

Fig. H1. Fraction of phosphorous present in vivianite as a function of the Fe/P molar ratio in the digested sludge of several WWTPs. Combined data from Wilfert et al., (2018) and the present study (data in Appendix H).5

Appendix I

To evaluate these phenomena, the ratio of the spectral contribution Site II/Site I as given by Mössbauer spectroscopy (Appendix B) can be used. At 300K, it has a value of 2 for pure vivianite, since 2 Fe^{2+} occupy the 2 octahedral sites II, while 1 Fe^{2+} occupies the octahedral site I (Mori and Ito, 1950). Manning et al., (1991) showed that divalent cations substitute preferentially in Site II, decreasing the ratio. On the contrary, oxidation should occur more easily in the site I, increasing the ratio (Rouzies and Millet, 1993; McCammon et al., 1980).

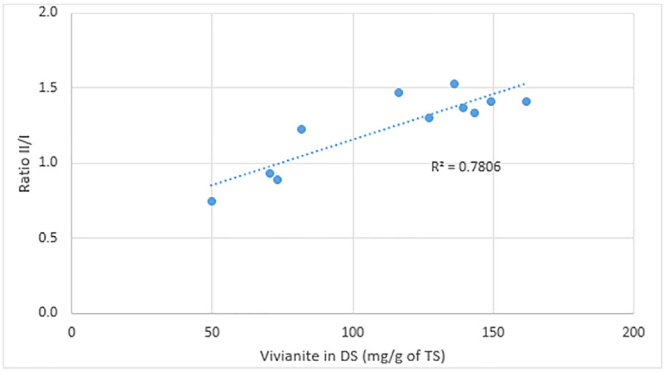

Fig. I1. Ratio between Site II and I as given by Mössbauer spectroscopy (Table B1), as a function of the vivianite content in the digested sludge of Nieuwveer

Interestingly, the ratio Site II/Site I increased with the vivianite content in sludge (Fig. I1). It can either suggest that the more vivianite in sludge, the more oxidized it is (1), or the more vivianite in sludge, the purer it is (2). We showed before that more vivianite was formed when the Fe dosing was higher. Under these conditions, the saturation index for the formation of vivianite should be higher, so we can hypothesize that more vivianite formed before digestion. This early-formed vivianite goes through oxidative conditions, and is, therefore, more likely to be oxidized, which goes in the direction of the case (1). However, the degree of oxidation as given by Mössbauer (Ratio $(Fe^{2+}I + Fe^{2+}II)/Fe^{3+}(I + II)$ in Table B1) stays constant with the vivianite content increase in DS, disproving the hypothesis (1). The amount of cations susceptible to replace Fe in vivianite (Ca & Mg were the most present) stayed constant in the DS. We could imagine that if there is more vivianite in sludge, the impurities substituting Fe should be more diluted in vivianite, supporting the hypothesis (2). While Fe dosing was increased, our team was also operating a pilot installation in Nieuwveer to magnetically extract vivianite from the DS (unpublished results). The extracted vivianite (purity 55–80%) was analyzed for cations concentrations to confirm (2). From the cations II present (Ca, Mg, Mn …), only Mg concentration was decreasing as vivianite content increased while the other cations were not showing clear trends (Appendix F).

Appendix J

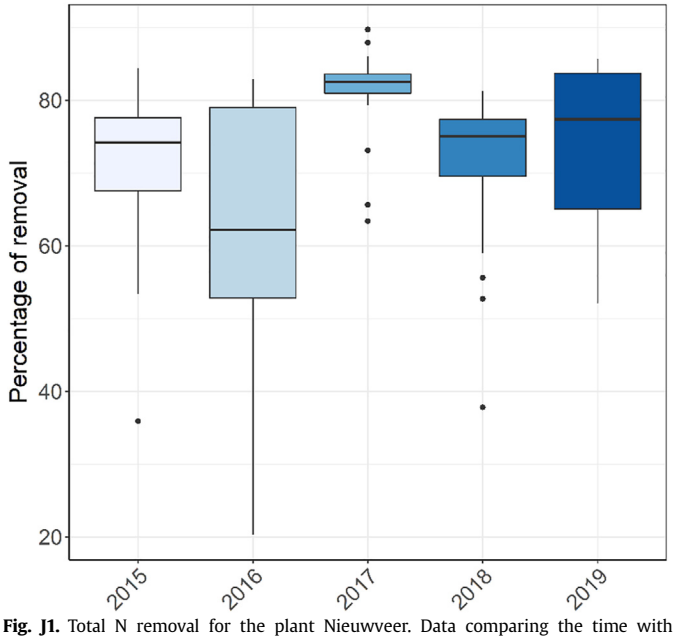

Fig. J1. Total N removal for the plant Nieuwveer. Data comparing the time with standard Fe dosing (2015–2018) to the time with doubled Fe dosing (2019) on the period January–April.

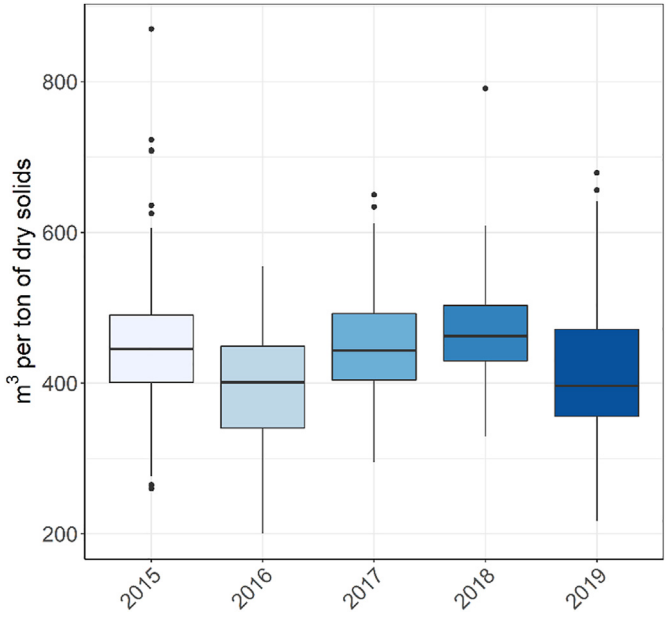

Fig. J2. Biogas production for the plant Nieuwveer. Data comparing the time with standard Fe dosing (2015–2018) to the time with doubled Fe dosing (2019) on the period January–April.

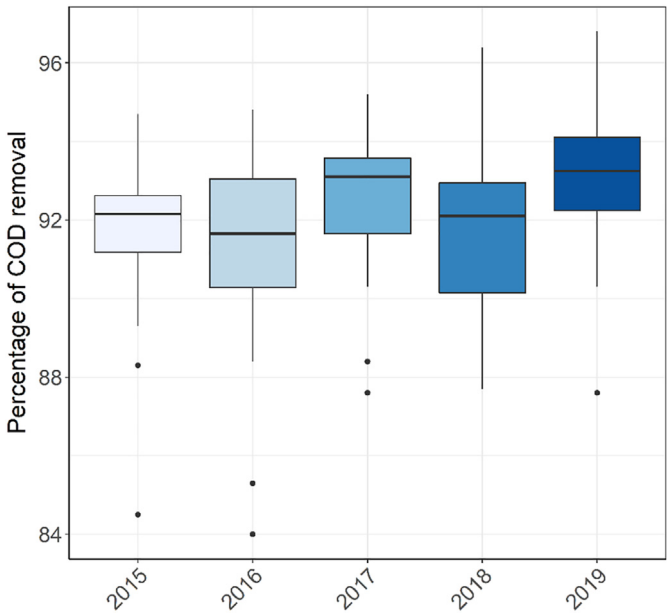

Fig. J3. N removal for the plant Nieuwveer. Data comparing the time with standard Fe dosing (2015–2018) to the time with doubled Fe dosing (2019) on the period January–April.

Appendix K

The following calculation show that the aeration energy necessary to fully oxidize the extra Fe dosed in Nieuwveer (366 kg/day) is negligible compared to the aeration necessary for the COD removal.

The equation of oxidation of Fe^{2+} into Fe^{3+} is:

$$4H^+ + O_2 + 4Fe^{2+} = 4Fe^{3+} + 2H_2O$$

It means that 1 mol of oxygen is necessary to fully oxidize 4 mol of Fe^{2+}. Calculations give that to oxidize 366 kg of Fe^{2+}, 52.5 kg of O_2 are necessary.

In the WWTP Nieuwveer, the average daily COD was 587 ppm O_2 for the period January–April 2019. The average flowrate on the same period being 76,273 m^3/day, it means that 44.8 tons of O_2 are necessary to entirely remove this COD. Considering that the plant COD removal is 93%, 41.7 tons of O_2 are used everyday to treat the COD.

It means that the O_2 that would be necessary to fully oxidize the extra Fe^{2+} dose represents 0.1% of the O_2 used for COD removal, which is negligible.

References

Čermáková, Z., Švarcová, S., Hradil, D., Bezdicka, P., 2013. Vivianite: a historic blue pigment and its degradation under scrutiny. In: Science and Technology for the Conservation of Cultural Heritage, pp. 75–78.

Abros'kina, D.P., Fuentesb, M., Garcia-Minab, J.M., Klyainc, O.I., Senikd, S.V., Volkova, D.S., Perminovaa, I.V., Kulikovaa, N.A., 2016. The effect of humic acids and their complexes with iron on the functional status of plants grown under iron deficiency. Eurasian Soil Sci. 49 (10), 1099–1108.

Al-Borno, A., Tomson, M.B., 1994. The temperature dependence of the solubility product constant of vivianite. Geochem. Cosmochim. Acta 58 (24), 5373–5378.

Bratby, J., 2016. Coagulation and Flocculation in Water and Wastewater Treatment, third ed.

Brown, M.E., Buchanan, K.J., Goosen, A., 1985. Thermodynamically and kinetically controlled products. J. Chem. Educ. 62 (7), 575.

Childers, D., Corman, J., Edwards, M., Elser, J., 2011. Sustainability challenges of phosphorus and food: solutions from closing the human phosphorus cycle. Bioscience 61 (2), 117–124.

Cordell, D., White, S.B., 2015. Tracking phosphorus security: indicators of phosphorus vulnerability in the global food system. Food Secur. 7 (2).

Cornel, P., Schaum, C., 2009. Phosphorus recovery from wastewater: needs, technologies and costs. Water Sci. Technol. 59 (6), 1069–1076.

Desmidt, E., Ghyselbrecht, K., Zhang, Y., Pinoy, L., Van der Bruggen, Bart, Verstraete, W., Rabaey, K., Meesschaert, B., 2015. Global phosphorus scarcity and full-scale P-recovery techniques: a review. Crit. Rev. Environ. Sci. Technol. 45 (4), 336–384.

Dewil, R., Baeyens, J., Roels, J., Van de Steene, B., 2009. Evolution of the total sulphur content in full-scale wastewater sludge treatment. Environ. Eng. Sci. 26 (4).

European Sustainable Phosphorus Platform, 2019. Report from of the "ESPP Waste Water Phosphorus Removal Workshop" from November 2019 Host. the University of Liège.

Frossard, E., Bauer, J.P., Lothe, F., 1997. Evidence of vivianite in FeSO4-flocculated sludges. Water Res. 31 (10), 2449–2454.

Gutierrez, O., Park, D., Sharma, K.R., Yuan, Z., 2010. Iron salts dosage for sulfide control in sewers induces chemical phosphorus removal during wastewater treatment. Water Res. 44 (11), 3467–3475.

Henze, M., Van Loosedrecht, M.C.M., Ekama, G.A., Brdjanovic, D., 2008. Biological Wastewater Treatment: Principles, Modelling and Design.

Klencsar, Z., 1997. Mössbauer spectrum analysis by evolution algorithm. Nucl. Instrum. Methods Phys. Res. Sect. B Beam Interact. Mater. Atoms 129 (4), 527–533.

Li, J., 2005. Effects of Fe(III) on floc characteristics of activated sludge. J. Chem. Technol. Biotechnol. 80 (3), 313–319.

Liu, J., Cheng, X., Qi, X., Li, N., Tian, J., Qiu, B., Xu, K., Qu, D., 2018. Recovery of phosphate from aqueous solutions via vivianite crystallization : thermodynamics and influence of pH. Chem. Eng. J. 349, 37–46.

Lovley, D.R., Blunt-Harris, E.L., 1999. Role of humic-bound iron as an Electron transfer agent in dissimilatory Fe(III) reduction. Appl. Environ. Microbiol. 65 (9), 4252–4254.

Mamais, D., Pitt, P.A., Cheng, Y.W., 1994. Determination of ferric chloride dose to control struvite precipitation in anaerobic sludge digesters. Water Environ. Res. 66 (7), 912–918.

Manning, P.G., Murphy, T.P., Prepas, E.E., 1991. Intensive formation of vivianite in the bottom sediments of mesotrophic Narrow Lake, Alberta. Can. Mineral. 29, 77–85.

McCammon, C.A., Burns, R.G., 1980. The oxidation mechanism of vivianite as studied by Mossbauer spectroscopy. Am. Mineral. 65 (3–4), 361–366.

Mersmann, A., 2001. Crystallization Technology Handbook, second ed. Revised and Expanded.

Mori, H., Ito, T., 1950. The structure of vivianite and symplesite. Acta Crystallogr. 3 (1), 1–6.

Morse, G.K., Brett, S.W., Guy, J.A., Lester, J.N., 1998. Review: phosphorus removal and recovery technologies. Sci. Total Environ. 212 (1), 69–81.

Nembrini, G.P., Capobianco, J.A., Viel, M., Williams, A.F., 1983. A Mössbauer and chemical study of the formation of vivianite sediments of Lago Maggiore (Italy). Geochem. Cosmochim. Acta 47 (8), 1459–1464.

Nielsen, A.H., Lens, P., Vollertsen, J., Hvitved-Jacobsen, T., 2005. Sulhide-iron interactions in domestic wastewater from a gravity sewer. Water Res. 39 (12), 2747–2755.

Nriagu, J.O., 1972. Stability of vivianite and ion-pair formation in the system $Fe_3(PO4)_2$-$H_3PO_4H_3PO_4$-H_2O. Geochem. Cosmochim. Acta 36 (4), 459–470.

Nriagu, J.O., Dell, C.I., 1974. Diagenetic formation of Iron phosphates in recent lake sediments. Am. Mineral. 59, 934–946.

Ogorodova, L., Vigasina, M., Mel'chakova, L., Rusakov, V., Kosova, D., Ksenofontov, D., Bryzgalov, I., 2017. Enthalpy of formation of natural hydrous iron phosphate: Vivianite. J. Chem. Thermodyn. 110, 193–200.

Ohtake, H., Tsunade, S., 2019. Chapter 1: Development of Phosphorus Recycling in Europe and Japan. *Phosphorus Recovery and Recycling*, pp. 3–27.

Pons, M.N., Spanjers, H., Baetens, D., Nowak, O., Gillot, S., Nouwen, J., Schuttinga, N., 2004. Wastewater Characteristics in Europe – A Survey. European Water Management Online.

Pourbaix, M., 1963. Atlas of Electrochemical Equilibria. Gauthier-Villars, Paris.

Prot, T., Nguyen, V.H., Wilfert, P., Dugulan, A.I., Goubitz, K., De Ridder, D.J., Korving, L., Rem, P., Bouderbala, A., Witkamp, G.J., Van Loosdrecht, M.C.M., 2019. Magnetic separation and characterization of vivianite from digested sewage sludge. Separ. Purification (224).

Rasmussen, H., Nielsen, P., 1996. Iron reduction in activated sludge measured with different extraction techniques. Water Res. 30 (3), 551–558.

Recham, N., Armand, M., Laffont, L., Tarascon, J.-M., 2009. Eco-efficient synthesis of LiFePO4 with different morphologies for Li-ion batteries. Electrochem. Solid State Lett. 12 (2), A39.

Rombolà, A.D., Toselli, M., Carpintero, J., Quartieri, M., Torrent, J., Marangoni, B., 2007. Prevention of iron - deficiency induced chlorosis in kiwifruit (actinidia deliciosa) through soil application of synthetic vivianite in a calcareous soil. J. Plant Nutr. 26 (10–11), 2031–2041.

Rosenqvist, I.T., 1970. Formation of vivianite in Holocene clay sediments. Lithos 3, 327–334.

Rothe, M., Kleeberg, A., Hupfer, M., 2016. The occurrence, identification and environmental relevance of vivianite in waterlogged soils and aquatic sediments. Earth Sci. Rev. 158, 51–64.

Rouzies, D., Millet, J.M.M., 1993. Mossbauer study of synthetic oxidized vivianite at room-temperature. Hyperfine Interact. 77 (1–2), 19–28.

Seitz, A., Riedner, J., Malhotra, K., Kipp, J., 1973. Iron-phosphate compound identification in sewage sludge residue. Environ. Sci. Technol. 7 (4), 354–357.

SNB Annual report (2018). (N.V. Slibverwerking Noord-Brabant).

Suresh Kumar, P., Korving, L., Van Loosdrecht, M.C.M., Witkamp, G.J., 2019. Adsorption as a technology to achieve ultra-low concentrations of phosphate: research gaps and economic analysis. Water Res. X, 4.
Viollier, E., Inglett, P.W., Hunter, K., Roychoudhury, A.N., van Cappellen, P., 2000. The ferrozine method revisited: Fe(II)/Fe(III) determination in natural waters. Appl. Geochem. 15 (6), 785–790.
Wang, R., Wilfert, P., Dugulan, I., Goubitz, K., Korving, L., Witkamp, G.J., Van Loosdrecht, M.C.M., 2019. Fe(III) reduction and vivianite formation in activated sludge. Separ. Purif. Technol. 220, 126–135.
Wilfert, P., Kumar, P.S., Korving, L., Witkamp, G.J., Van Loosdrecht, M.C.M., 2015. The relevance of Phosphorus and iron chemistry to the recovery of phosphorus from wastewater. Environ. Sci. Technol. 49 (16).
Wilfert, P., Mandalidis, A., Dugulan, A.I., Goubitz, K., Korving, L., Temmink, H., Witkamp, G.J., Van Loosdrecht, M.C.M., 2016. Vivianite as an important iron phosphate precipitate in sewage treatment plants. Water Res. 104, 449–460.
Wilfert, P., Korving, L., Dugulan, I., Goubitz, K., Witkamp, G.J., Van Loosdrecht, M.C.M., 2018. Vivianite as the main phosphate mineral in digested sewage sludge and its role for phosphate recovery. Water Res. 144, 312–321.
Zelibor, J.L., Senftle, F.E., Reinhardt, J.L., 1988. A proposed mechanism for the formation of spherical vivianite crystal aggregates in sediments. Sediment. Geol. 59 (1–2), 125–142.